ISTANBUL TECHNICAL UNIVERSITY ★ GRADUATE SCHOOL OF SCIENCE ENGINEERING AND TECHNOLOGY

FABRICATED OF FE-RICH AND TI-RICH OXIDE ANODE MATERIALS FROM FERROTITANIUM FOR LITHIUM ION MATERIALS

M.Sc. THESIS

EREN İNEL

Department of Metallurgical and Materials Engineering

Material Engineerings Programme

SEPTEMBER 2019

ISTANBUL TECHNICAL UNIVERSITY ★ GRADUATE SCHOOL OF SCIENCE ENGINEERING AND TECHNOLOGY

FABRICATED OF FE-RICH AND TI-RICH OXIDE ANODE MATERIALS FROM FERROTITANIUM FOR LITHIUM ION MATERIALS

M.Sc. THESIS

EREN İNEL
(506171410)

Department of Metallurgical and Materials Engineering

Materials Engineerings Programme

Thesis Advisor: Prof. Dr. Özgül KELEŞ
Thesis Co-Advisor: Assist. Prof. Dr. Billur Deniz KARAHAN

SEPTEMBER 2019

ISTANBUL TEKNİK ÜNİVERSİTESİ ★ FEN BİLİMLERİ ENSTİTÜSÜ

DEMİRCE ZENGİN VE TİTANYUMCA ZENGİN OKSİT ANOT MALZEMELERİN FERRO-TİTANYUM ALAŞIMINDAN ELDESİ VE LİTYUM İYON BATARYALARDA KULLANIMLARI

YÜKSEK LİSANS TEZİ

EREN İNEL
(506171410)

Metalurji ve Malzeme Mühendisliği Anabilim Dalı

Malzeme Mühendisliği Programı

Tez Danışmanı: Prof. Dr. Özgül KELEŞ
Eş Danışman: Dr. Öğr. Üye. Billur Deniz KARAHAN

EYLÜL 2019

Eren İNEL, a M.Sc. student of ITU Graduate School of Science Engineering and Technology student ID 506171410, successfully defended the thesis entitled "FABRICATED OF FE-RICH AND TI-RICH OXIDE ANODE MATERIALS FROM FERROTITANIUM FOR LITHIUM ION MATERIALS", which he prepared after fulfilling the requirements specified in the associated legislations, before the jury whose signatures are below

Thesis Advisor :	**Prof. Dr. Özgül KELEŞ** Istanbul Technical University	.....
Co-advisor :	**Assist. Prof. Dr. Deniz KARAHAN** Istanbul Medipol University	.....
Jury Members :	**Prof. Dr. Gültekin GÖLLER** Istanbul Technical University	.....
	Prof. Dr. Sebahattin GÜRMEN Istanbul Technical University	.....
	Assoc. Prof. Dr. Rezan DEMİR ÇAKAN Gebze Technical University	.....

Date of Submission : 05 September 2019
Date of Defense : 06 September 2019

To my family,

FOREWORD

First of all I want to thank my thesis advisor, Prof. Dr. Özgül KELEŞ for her support, motivation and guidance during this thesis.

I sincerely thank to my co-advisor Assist. Prof. Dr. Deniz KARAHAN for her continuous support and motivating attitude.

I would like to express my thanks to Prof. Dr. Gültekin GÖLLER for giving me the permission of using the equipments of Biomaterial laboratory and also thank to Research Assistants Barış YAVAŞ for his kind help that he offered during XRD analysis.

I would like to thank Prof. Dr. Sebahattin GÜRMEN for giving me permission to use grinding machine.

I would like to thank academic members of Faculty of Engineering and Natural Science at Istanbul Medipol University, Assoc. Prof. Dr. Yasemin Yüksel DURMAZ, Research Assistant Erhan DEMİREL and Ezgi KARACA.

I would like to thank my lab partners, Research Assistant İpek TUNÇ, Dila SİVLİN, Reyhan SOLMAZ and Barış Cem ALPAY for their kindnesses and infinite friendships. In addition I would like to Dr. Halim POLAT, Sefa ÇINAR and Aylin KARACA from Galtek Galvano Ltd. Şti for helping me to accomplish my experimental studies and characterizations on time.

I would like to thank Bora TARHAN and Marmara Metal Mamulleri Tic. A.Ş. for their helping.

I would like to thank my family for their endless support and love.

September 2019

Eren İNEL
Metallurgical and Materials Engineer

TABLE OF CONTENTS

Page

ABBREVIATIONS

LIB **:** Lithium- Ion Battery
EC **:** Ethylene Carbonate
DEC **:** Diethyl Carbonate
DMC **:** Dimethyl Carbonate
CV **:** Cyclic Voltammetry
EIS **:** Electrochemical Impedance Spectroscopy
SEI **:** Solid Electrolyte Interface
PVDF **:** Polyvinylidene Difluoride
NMP **:** N-Methylpyrrolidone
TMO **:** Transition Metal Oxide
XRD **:** X-Ray Diffraction
SEM **:** Scanning Electron Microscope
EDS **:** Energy Dispersive X-ray Spectroscopy
AAS **:** Atomic absorption spectroscopy

SYMBOLS

ºC : Celsius

EV : Electrical Vehicles

BEV : Battery Electrical Vehicles

nm : Nanometer

µm : Micrometer

Hz : Hertz

kHz : Kilo hertz

V : Voltage

LIST OF TABLES

Page

LIST OF FIGURES

Page

FABRICATED OF FE-RICH AND TI-RICH OXIDE ANODE MATERIALS FROM FERROTITANIUM FOR LITHIUM ION MATERIALS

SUMMARY

In recent years, environmentally friendly, renewable energy resources become an important subject because the great damages caused by the fossil fuels risk sustainable life for future. Research on this subject not only covers the production of green energy but its transportation and storage as well. In this perspective, studies of secondary batteries are prevalent as they provide power to portable devices, electric vehicles and energy grids. Among alternatives, lithium ion secondary batteries attract attention due to their high energy densities, long cycle life and environmental friendliness.

LIBs are composed of positive and negative electrodes, electrolyte and separator components. Positive and negative electrodes are the most important components that determine the characteristics of the battery. The cathode (positive electrode) delivers Li ions and the anode (negative electrode) accommodates them depending on its structural features. The electrolyte is a medium in which Li ions can easily ring between the anode-cathode. The separator material is an insulating polymer material to prevent short circuit between the positive and negative electrodes. In charging, Li ions that are coming out of the cathode material intercalates into the anode material and the energy is stored. Then, in discharging this energy is realesed following the requirements, while Li ions are deintercalated into its host material (cathode).

History shows that the world's energy shortage in 1960 led the introduction of Li batteries into the energy sector. First, primary Li batteries were used as an energy source where metallic Li was used as anode and titanium sulphide as cathode material. Then, Goodenough et. al proposed the use of $LiCoO_2$ (Li containing host material) as cathode and graphite as anode material to design secondary lithium ion batteries. This design enables the intercalation/deintercalation of Li ions in cycling. Therefore, the battery could be used multiple times by recharging. In 1991, Sony produced first commercial secondary Li batteries. However, due to the low energy density of graphite (372 mAh/g) the battery was enable to meet the increasing energy needs of consumers. Therefor, search for alternative anode materials has gained speed. As a result, tin (Sn), antimony (Sb), aluminum (Al), silicon (Si), bismuth (Bi) and metal oxide type materials were considered to replace to the state-of-the-art anode, graphite.

The competition in the market not only requires producers to extend the energy and power densities of the batteries but also enforce them to reduce the production cost. Therefore, researchers are working to find an appropriate approach to fabricate high energy-density electrode materials via a sustainable, green and affordable method. Since the price of raw material is of critical importance in the production cost, processes in which domestic products are used as raw materials should be developed.

On the other hand, currently the raw materials of the electrodes used in secondary battery technology are obtained as a result of heavy mining processes. Wastes from mining and mine processing often lead many researchers to question the environmentally friendly approach of this battery technology. In this case, it is important to fabricate electrode material which is accepted as a high-value-added product by using domestic products as starting materials.

In this study, metal oxide anode material with high energy efficiency and long cycle life is aimed to be developed by using a domestic product as the raw material of the designed process. The originality of this study lies in the use of ferrotitanium alloy as the starting material for the production of anode material. Iron-titanium alloy is prefered not only it is a domestic intermediate product, but also it contains high amount of iron and titanium along with aluminum, magnesium. Indeed, literature reveals that iron oxide and titanium oxide powders are widely used as electrode materials and possible impurities in the oxide structure may improve the electrochemical performances of these electrodes.

Upto now, an analysis about the electrochemical performances of the iron oxide and / or titanium oxide powders that are selectively recovered from the acid leaching of iron-titanium alloy has not been published yet. First, in the open literature, in this thesis, first titanium oxide then iron oxide powders are recovered sepearately from ferro-titanium alloy and their possible uses as anode materials have been discussed. The fact that no need to use highly pure chemistry and expensive starting material for the production of transition metal oxide powders make this thesis interesting and promising. Plus, by using ferrotitainum alloy as the starting material, the destructive effect of green house emission issued by the traditional production step (mining, pyrometallurgy etc) is aimed to be minimized.

This thesis unifies extractive metallurgy and electrochemistry principles to construct a new method for the fabrication of anode material that may be used in lithium ion batteries. In the context of the study grinding, leaching and calcination are used to fabricate oxide powders as semi- products. Then, they are laminated for the fabrication of anode, as the final product. Both semi and final products will be characterized morphologically, chemically, structurally and electrochemically. In leaching process, sulfuric acid is used to selectively etch iron ions from ferro titanium alloys. Taguchi experimental design approach is used to understand the leaching parameters' effects on the leaching efficiency of iron ions and the titanium oxide powders. Within the experimental procedure first titanium ions are recovered as titanium oxide powders; then from the leachate iron oxalate are precipitated as a result of the oxalic acid reaction with leachate solution. The use of these oxide powders as anode material for lithum ion batteries have been investigated based on their galvanostatic and electrochemical performances.

The results show that sulfuric acid is an effective agent to leach ferrotitanium alloy. L_9 Taguchi experimental design has been used in the experiments. The most effective parameters to maximize the weight of titanium oxide and iron ion leaching efficiency are molar of acidic solution and solid/liquid ratio, respectively. The electrochemical test results show that sample 7 of titanium oxide powder that produced under condition 3 M acid concentration, 80^0C temperature, 1/25 solid/liquid ratio and 3 h leaching time, peforms the highest initial capacity (700 mAh/g) and capacity retention (35%) due to nano-sized spheres of regular morphology and narrow-size distribution. Spherical morphology increasing the active surface with the electrolyte

and complex metal oxide particles presence in the structure are believed to increase the capacity of the sample. For iron oxide powders, Sample 7 (3 M acid concentration, 80^0C temperature, 1/25 solid/liquid ratio and 3 h leaching time) delivers highest initial capacity (2100 mAh/g) and sample 4 that is carried out under 0.5 M acid concentration, 80^0C 1/100 solid/liquid ratio and 6 h leaching time, show the highest capacity retention (%34). The rod-like morphology of the sample increasing the contact area of the eletrode and the existence of impurities' complex oxide particles may elucidate this performance.

The idea behind the thesis is very unique. The results are found to be promising. It is believed that this study will open new gates for scientists who will work on engineering novel electrodes for next generation batteries.

DEMİRCE ZENGİN VE TİTANYUMCA ZENGİN OKSİT ANOT MALZEMELERİN FERRO-TİTANYUM ALAŞIMINDAN ELDESİ VE LİTYUM İYON BATARYALARDA KULLANIMLARI

ÖZET

Sanayi devriminden sonra artan sanayileşme ve hayat standartları, dünyada enerji kullanımı önemli derecede arttırmıştır. Özellikle elektrik enerjisi, modern sanayinin ve insan yaşamının vazgeçilmez unsurlarından biri olmuştur. Dünyada üretilen elektrik enerjisinin %80'i fosil yakıtlardan sağlanmaktadır. Son yıllarda fosil yakıtların, sürdürülebilir bir çevreye ve yaşama olan zararları artması nedeniyle, çevre dostu ve yenilenebilir enerji kaynakları önemli bir araştırma konusu olmuştur. Bu konudaki araştırmalar sadece yeşil enerji üretimini değil aynı zamanda taşınımını ve depolanmasını da kapsamaktadır. Enerji üretimindeki aksaklıklar, sanayide birçok problemi beraberinde getirmektedir. Ayrıca günlük hayatta kullanılan taşınabilir aygıtların ve elektrik enerjisi ile çalışan araçların sayısının artması nedeniyle, enerjiyi depolama konusunda yapılan çalışmalar son yıllarda hız kazanmıştır. Bu açıdan bakıldığında, ikincil piller üzerine yapılan çalışmalar, taşınabilir aygıtlara, elektrikli taşıtlara ve enerji ızgaralarına güç sağladıkları için oldukça yaygınlaşmıştır. Alternatifler arasında, lityum iyon ikincil piller, yüksek enerji yoğunlukları, uzun kullanım ömrü ve çevre dostu olmaları nedeniyle dikkat çekmektedir.

LIB'ler pozitif ve negatif elektrot, elektrolit ve seperatör bileşenlerden oluşur. Pozitif ve negatif elektrotlar, bataryanın özelliklerini belirleyen en önemli bileşenlerdir. Katot (pozitif elektrot) iyonları iletir ve anot (negatif elektrot) yapısal özelliklerine bağlı olarak bu iyonları yapılarında depolarlar. Elektrolit, Li iyonların anot ve katot arasında kolayca hareket edebileceği bir ortamdır. Ayırıcı malzeme, pozitif ve negatif elektrotlar arasındaki kısa devreyi önlemek için polimer malzemelerinden üretilmektedir. Şarj işlemi sırasında, katot malzemesi ortama aktif iyon sağlayan kaynak görevi üstlenir. Katotdan gelen Li iyonları anot malzemesi ile karşılaşır ve malzeme yapısının el verdiği kadar yapı içerisine girerler ve enerji depolanır. Daha sonra deşarj sırasında, Li iyonları cathod malzemesinin yapısından çıkarak katota doğru hareketlerini gerçekleştirirler ve bu sırada gerekli miktardaki enerji ortama sağlanmış olur.

Tarihde, 1960 yılında dünyada yaşanan enerji kıtlığı, Li pillerin enerji sektörüne girmesine yol açtığını gösteriyor. İlk olarak, birincil Li piller, metalik Li'nin anot ve titanyum sülfat malzemesinin katot olarak yer aldığı bir enerji kaynağı olarak kullanılmıştır. Daha sonra, Goodenough ve arkadaşları, ikincil lityum iyon pilleri tasarlamak için $LiCoO_2$'nin (Li içeren konakçı malzeme) katot ve grafit olarak anot malzemesi olarak kullanılmasını önermiştir. Bu tasarım Li-iyonların anot-katot çevrimi sırasında araya girme/aradan çıkma (intercalation/deintercalation) mekanizmasına olanak sağlar. Bu nedenle, pil şarj edilerek birden çok kez kullanılabilir. 1991'de Sony ilk ticari ikincil Li pilleri üretmiştir. Bununla birlikte, grafitin (372 mAsa/g) düşük enerji yoğunluğu ve artan enerji ihtiyaçlarını

karşılayamama nedeniyle, alternatif anot malzemelerinin aranması hız kazanmıştır. Sonuç olarak, Kalay (Sn), antimon (Sb), alüminyum (Al), silikon (Si), bizmut (Bi) ve metal oksit tipi malzemelerin en son teknolojiye sahip anot grafit yerine kullanılmaları düşünülmektedir.

Günümüzde batarya piyasasında arta rekabet sebebiyle üreticilerin batarya maliyetlerini düşürmelerini gerekli kılmaktadır. Bu nedenle, araştırmacılar sürdürülebilir, yeşil ve uygun maliyetli bir yöntemle yüksek enerji yoğunluklu elektrot malzemesini üretmek için uygun bir yaklaşım bulmak için çalışmaktadırlar. Hammadde fiyatı üretim maliyetinde kritik öneme sahip olduğundan, ucuz yerli ürünlerin hammadde olarak kullanıldığı süreçler geliştirilmelidir. Ayrıca gelişmekte ve dışa bağımlı olan ülkelerde ülkelerde, yerli hammaddelerden üretilen katma değeri yüksek ürünler, ülke ekonomisi için hayati öneme sahiptir. Bu durumda, katma değeri yüksek ürünler olarak kabul edilen elektrot malzemesinin üretiminde başlangıç malzemesi olarak yerli hammaddelerin kullanılması önemli bir konu haline gelmektedir.

Öte yandan, günümüzde ikincil batarya teknolojisinde kullanılan elektrotların hammaddeleri, ağır madencilik süreçlerinin bir sonucu olarak elde edilmektedir. Madencilik ve maden işleme atıkları, çoğu araştırmacının, bu pil teknolojisinin çevre dostu yaklaşımını sorgulamasına neden olmaktadır.

Bu çalışmada, yüksek enerji verimliliği ve uzun çevrim ömrüne sahip metal oksit anot materyali, tasarlanan işlemin hammaddesi olarak bir yerli ürün kullanılarak geliştirilmesi amaçlanmıştır. Bu çalışmanın orijinalliği, anot malzemesinin üretimi için başlangıç maddesi olarak ferrotitanyum alaşımının kullanılmasıdır. Demir-titanyum alaşımı sadece yerli bir ara ürün değildir, aynı zamanda alüminyum, magnezyum ile birlikte yüksek miktarda demir ve titanyum içerir. Aslında, literatür taraması, demir oksit ve titanyum oksit tozlarının, elektrot malzemesi olarak yaygın şekilde kullanıldığını ve oksit yapısındaki olası kirliliklerin, bu elektrotların elektrokimyasal performansını artırabileceğini ortaya koymaktadır.

Şimdiye kadar demir-titanyum alaşımının asit liçinden seçilen selektif olarak geri kazanılan demir oksit ve/veya titanyum oksit tozlarının elektrokimyasal performansları hakkında bir analiz henüz yayınlanmamıştır. İlk önce, bu tezde titanyum oksit, ardından demir oksit tozları ferro-titanyum alaşımından geri kazanılmış ve anot malzemeleri olarak kullanımları tartışılmıştır. Geçiş metal oksit tozlarının üretimi için yüksek saflıkta kimyasala ve pahalı başlangıç malzemesi kullanmaya gerek olmaması bu tezi ilginç ve umut verici kılmaktadır. Ayrıca, başlangıç materyali olarak ferrotitanyum alaşımı kullanılarak, geleneksel üretim yöntemleri (madencilik, pirometalurji vb.) tarafından üretilen sera gazı emisyonlarının yıkıcı etkisinin en aza indirilmesi amaçlanmaktadır. Çalışma 'sıfır atık' ilkesi çerçevesinde gerçekleştirilmeye çalışarak, çevreye zararsız üretim süreci geliştirilmesi hedeflenmiştir.

Bu tez, lityum iyon pillerde kullanılabilecek anot malzemesinin üretimi için yeni bir yöntem inşa etmek için ekstraktif metalurji ve elektrokimya prensiplerini birleştirmektedir. Çalışma kapsamında, öğütme, liç ve kalsinasyon, oksit tozlarını yarı mamül olarak üretmek için kullanılmıştır. Daha sonra, son ürün olarak anot üretimi için lamine edilmişlerdir. Hem yarı hem de nihai ürünler, morfolojik, kimyasal, yapısal ve elektrokimyasal tekniklerle karakterize edilmişlerdir. Liç işleminde, demir iyonlarını ferrotitanyum alaşımlarından seçici olarak almak için sülfürik asit kullanılmıştır. Taguchi deneysel tasarım yaklaşımı, liç parametrelerinin

'demir iyonlarının liç verimliliği ve demir oksit tozu morfolojisi üzerindeki etkilerini anlamak için kullanılmıştır. Deneysel prosedürde, titanyum iyonları da titanyum oksit tozları olarak geri kazanılmıştır. Daha sonra, bu oksit tozlarının, lityum iyon piller için anot malzemesi olarak kullanımı, galvanostatik ve elektrokimyasal performanslarına dayanılarak incelenmiştir.

Sonuçlar gösteriyor ki, sulfürik asit, ferrotitanyum alaşımının liç işleminde kullanılabilecek etkili bir ajandır. Deneylerde, $L_9(3^4)$ Taguchi deneysel tasarımı kullanılmıştır. Taguchi analizine göre, titanyum oksit tozlarını maksimum ağırlıkta üretmek için en etkili parametre asit molar miktarı iken, demir iyonlarının liç veriminde en etkili parametre, katı/sıvı oranı olarak belirlenmiştir. Elektrokimyasal analizlere göre titanyum için, 3 M asit konsantrasyonu, 80^0C sıcaklık, 1/25 katı/sıvı oranı ve 3 saat liç süresi parametreleri ile (numune 7) ve 0.5 M asit konsantrasyonu 120^0C sıcaklık, 1/50 katı/sıvı oranı ve 3 saat liç süresi parametreleri ile gerçekleştirilen (numune 6) deneylerden üretilen tozlar, nanometre seviyesinde küresel partiküllere ve karmaşık metal oksit formları içermelerinden dolayı, en yüksek başlangıç kapasitesine(700 mAsa/g) ve kapasite korumaya (%35) sahiptirler. Demir için ise, 3 M asit konsantrasyonu, 80^0C sıcaklık, 1/25 katı/sıvı oranı ve 3 saat liç süresi parametreleri ile (numune 7) elde edilen tozlar, en yüksek başlangıç kapasitesi (2100 mAsa/g) ve 0.5 M asit konsantrasyonu, 80^0C sıcaklık, 1/100 katı/sıvı oranı ve 6 saat liç süresinde (numune 4) elde edilen tozlar ise en yüksek kapasite korumaya (%34) sahiptirler. Demir oksit tozlarının sahip oldukları nano-çubuk yapıları elektrot aktif yüzey alanını arttırmış ve ayrıca, yapısında bulunan karmaşık oksit formdaki empurite elementleri, anot performansında olumlu etki göstermişlerdir.

Elde edilen sonuçlar gösteriyor ki, bu tezde işlenen fikir kendine özgüdür. Bu tezin, yeni nesil batarya teknolojileri üzerinde çalışan araştırmacılar için, yeni ve özgün konulara ışık tutacağına inanılmaktadır.

1. INTRODUCTION

Today, energy and green house emission become the major issues of the World. Recently, researchers have been focus to create and develop new energy technologies to alleviate enviromental problems that fossil fuel have caused [1]. Alternative use of renewable energy as energy resources has gained remarkable importance. Herein, beside fabrication, storage and transportation of this energy should be also improved to maximize its efficiency [2].

Lithium ion battery (LIB) are considered to be a promising energy storage device due its high energy density, high working potential, no memory effect and long cycle life. LIB are widely used in electrical vehicles, portable electronics for home appliances and electrical devices for medical and/or defense applications. Knowing that the development of the electrical vehicles (EVs) could represent a solution to decrease the green house gases emission, many researchers have been working to maximize the efficiency of the energy storage units of the EVs, named as 'batteries' by re-designing electrodes, the cell and their working conditions [3-5].

LIBs consist of oppositely charged electrodes (anode and cathode), seperator and electrolyte. In Li-ion cell, the main chemical reactions are reversible and should be occurred between the two electrodes following the intercalation/deintercalation of Li-ions [6,7].

When the history of LIBs are investigated, it is seen that at 1970s, firstly the primary Li battery was discovered. However, due to the high risk of explosion which might be occurred when Li gets in contact with oxygen (in air), safety became a big concern for batteries [8]. Then, in 1990, Sony has proposed a new technology: secondary Li-ion battery. It could be used over and over as much as Li ion is allowed to be intercalated/deintercalated morphologically and structurally. Herein, $LiCoO_2$ and graphite were used as the cathode and the anode materials [9].

However, due to the hazardous effect of the Co on human health, $LiFePO_4$ was proposed to be replaced with $LiCoO_2$ [10,11]. After this technological progress,

many alternative electrodes materials have been investigated and still continued to be studied until the best will be found [11].

Over the past years, United States, China and European countries have proceed with an acceleration in the field of battery technology. Today, thanks to the large companies that have been generously fund R&D activities on designing a low cost and better performance LIB, electrical vehicles become a big part of our life. There are almost 1.2 million electrical vehicles on the road of China and 750,000 on the road of the United States [12].

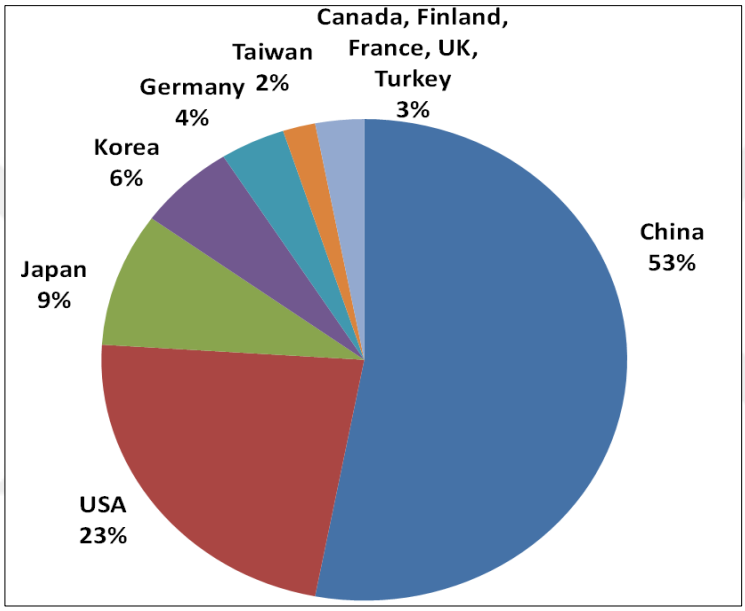

Figure 1.1 : Lithium ion battery production in the world [13].

In the next few years, many newly designed, low-cost batteries are expected to be commercialized. By 2023, prices are expected to become around USD 140 per kWh from the current USD 209 per kWh. Global Lithium-Ion Battery Market is considered to reach $56 billion by 2024 [13].

Today, there are 9 companies which are registrated to fabricate lithium ion batteries in world wide scale. In 2017, Contemporary Amperex Technology (CATL) produced 11.8 GWh of battery capacity CATL is the largest manufacturer of LIB with a capacity of 12 GWh. Japan's Panasonic was the second largest producer with 10 GWh, and BYD was third with 7.2 GWh. Another China-based producer, Optimum Nano Energy Co. Ltd., and South Korea's LG Chem were fourth and fifth on the list as they produced 5.5 GWh and 4.5 GWh, respectively. However, in Turkey there is no company which produces lithium ion batteries by using their own electrodes [13].

The idea behind this study is to unify extractive metallurgy and electrochemistry to fabricate electrodes of green energy storage devices with an environmentally friendly approach. In this perspective, first a domestic ferro-titanium alloy is leached with sulfuric acid. L_9 (3^4) Taguchi design of experiment has been used to analyze the process parameters (temperature, solid/liquid ratio, molar of acid and leaching time) on the leaching efficiency and achieve the highest productiveness eventually. In the second part, the recovered oxides (iron oxide and titanium oxide) are characterized structurally, compositionally and morphologically. The possible uses of these powders as anode material have been discussed based on electrochemical performances.

2. LITERATURE REVIEW

2.1 Lithium Ion Batteries

The first Li battery was born in the mid-1960s when pure Li metal was used as an anode material. The pure Li metal has a low molecular weight (6.941 g mol^{-1}) and density (0.51g cm^{-3}). Li metal has 3860 mAh/g specific capacity and high electro chemical potential (3V vs H/H^{+}) [1]. Therefore, Li-ion batteries have been attracted attention as they supply the energy demands of popular devices such as mobile phones, computers, tablets, electronic watchs, toys and also electrical vehicles [2]. Table 2.1 show that the some example of rechargeable batteries and their properties.

Table 2.1 : Rechargeable Batteries [3].

Battery	Energy Density (Wh/kg)	Theoritical Capacity (Ah/kg)	Cell Voltage (V)
Lead- Acid	30- 50	83	2
Ni-Cd	45- 80	162	1.2
NiMH	60- 120	178	1.2
Li-ion ($LiMnO_2$/graphite)	100- 150	104	3.7
Li-ion ($LiCoO_2$/graphite)	150- 250	158	3.6
Li-ion ($LiFePO_4/Li_4Ti_5O_{12}$)	90- 120	117	3.2- 3.3

To benefit the advantage of lithium and re-use the battery over and over, lithium ion batteries have been invented [4]. Rechargeble Li-ion battery consists of anode (negative electrode), cathode (positive electrode), electrolyte and seperator [5].

During the charge/discharge process, Li insertion/extraction processes take place between the negative and the possitive electrodes. This insertion/extaction process is reversible. Among the alternatives energy storage devices (such as nickel-cadmium,

lead- acid and nickel-metal hydrid batteries) Li-ion batteries provide higher energy density and longer cycle life. But, Li metal is highly reactive with air and water. Thus, after some fire incidents and explosion, the safety of battery in long cycle becomes the most significant drawback of this technology [6].

2.2 Working Principles of LIBs

The working principles of Li-ion batteries are based on electrochemical reaction between possitive and negative electrodes. The cathode materials generally compose of Li metal oxide and they serve as a Li source in batteries when charging. The anode materials accomodate lithium ions upon charging [7]. The secondary Li-ion batteries may include liquid or solid electrolyte where Li ions can pass through, but the electrons do not. In the cell design, the electrodes are seperated from each other by a porous seperator that is made of polyethylene or polypropylene material. Figure 2.1 show the working princible of the Li-ion batteries.

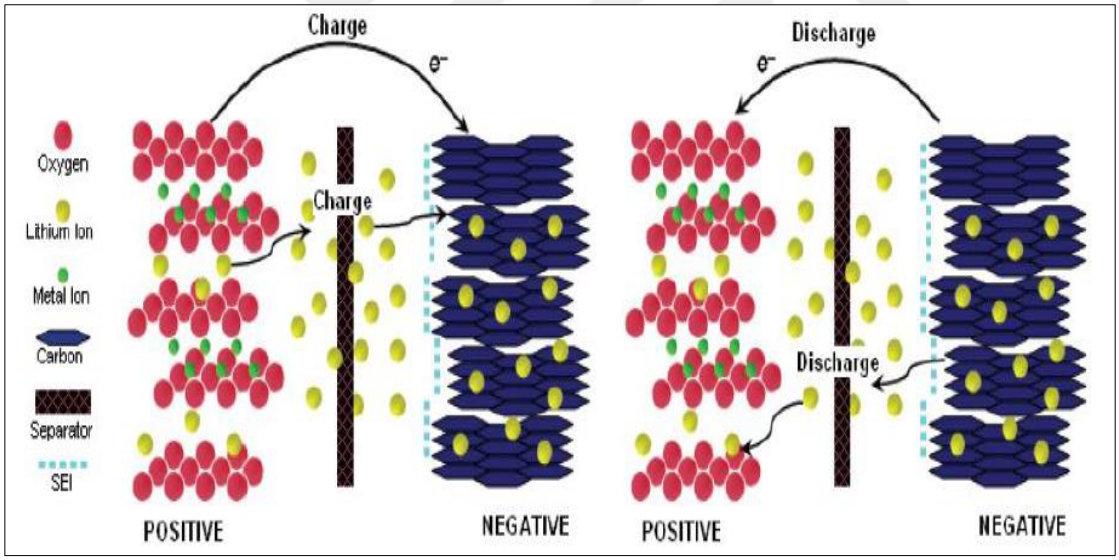

Figure 2.1 : Charge/discharge process of LIBs [8].

In charging, Li ions are deintercalated from the cathode material and pass through the electrolyte to enter into the crystal structure of anode materials. At the same time, the electrons move the same direction through an external wire. In the case of discharging, lithium ions are intercalated into the cathode material [7,9].

2.3 LIB Components

2.3.1 Electrolyte

Electrolyte serves as a medium which supports the movement of Li ions from the cathode to the anode then vice-versa in cycling. The electrolyte could be in solid or liquid phase. The liquid electrolytes typically are made of organic solvent and inorganic –orgainc salts. High chemical stability, high ionic conductivity, cost-effectiveness and safety are the major requisites of the electrolyte. As LIB working potential is above 3V and water becomes dissociated at this potential, organic liquids which include dissolved organic Li salts (such as $LiPF_6$) are considered as a possible electrolytes. To enhance the stability of the liquid electrolytes, carbonate (Ethylene carbonate (EC) and dimethyle carbonate (DMC) is added into the solution. [5,10,11].

Table 2.2. gives a comparison of some electrolytes used in LIBs [5]

Table 2.2 : Properties of some electrolyte[5].

Electrolyte	Boiling point (˚C)	Melting point (˚C)	Density (g/ml)	Viscosity (cP)	Molecular weight (g)	Dielctric constant
EC	248	39	1.41	1.86	88.1	89.6
DMC	90	4	1.07	0.59	90.1	3.12
DEC	126	-43	0.97	0.75	118.1	2.82
EMC	109	-55	1	0.65	104.1	2.9
PC	242	-48	1.21	2.5	102.1	64.4

2.3.2 Seperator

To prevent the short circuit between the anode and the cathode, seperator material has a big importance in LIB. Generally seperators are made of porous material that selectively allows Li ions passage through it. Chemical, thermal and mechanical stability of the seperator are very important for the performance of LIBs. In commercial applications, polyethyelene and polypropylene have been used as seperator materials [3,12].

2.3.3 Positive electrode

In the Li-ion battery, the source of the Li is the cathode material. The requisites of the cathode materials are as follows: safe, affordable in price, high structural stability, good electron conductivity, not soluble into the working electrolyte and high Li reaction voltage [13].

The material used as positive electrodes in LIBs are classified depending on the lithium intercalation dimension: olivine (1D), layered (2D) and spinel (3D). Table 2.3 [13] gives a comparison among olivine, layered and spinel structured cathode materials' specific capacities, volumetric capacities and lithiation potential values.

Table 2.3 : Electrochemical properties of some cathode materials [13].

Structure	Chemistry	Specific capacity(mAh/g) (theorical/observed)	Volumeric Capacity (mAh/cm^3) (theorical/observed	Potential vs. Li^+/Li
Layered	$LiCoO_2$	273/160 [14]	1363/550	3.9
	$LiNiO_2$	274/180[15]	1280	3.6
	$LiNi_xCo_yMn_zO_2$	270/150-180[13]	1333/600	3.8
	$LiNi_xCo_yAl_zO_2$	250/180[16]	1284/700	3.7
	$LiMnO_2$	285/140[17]	1148	3.3
	Li_2MnO_3	458/180[18]	1780	3.8
Spinel	$LiMn_2O_4$	148/120[19]	596	4.1
	$LiCo_2O_4$	142/84[20]	704	4.0
Olivine	$LiFePO_4$	170/165[21]	589	3.4
	$LiMnPO_4$	171/168[22]	567	3.8
	$LiCoPO_4$	167/125[23]	510	4.2
	$LiFeSO_4F$	151/120[24]	487	3.7
Tavorite	$LiVPO_4F$	156/129[25]	484	4.2

2.3.4 Negative electrode

Anode is named as the negative electrode of Li-ion batteries. The requisites from the anode material are as follows: safe, affordable in price, high structural stability, good

electron conductivity, not soluble into the working electrolyte and low Li reaction voltage.

Li-metal was used as the first commercial anode materials in Li batteries due to its low weight and high specific capacity. Then, scientists replaced Li by graphite in the cell because of the safety concerns. The long cycle life, relatively low cost and abundant material supply of carbon based materials make them, an attractive anode material for Li-ion batteries. In this sense, carbon nanofibers (450 mAh/g), carbon nanotubes (1100 mAh/g), graphene (960 mAh/g), graphite (375mAh/g) and porous carbon (800–1100 mAh/g) have been studied as anode material of LIBs. It is noteworthy that very low lithiation potential that may cause short circuit in the cell becomes a major concern for the use of graphite in LIBs. Moreover, the restricted amount of the capacity delivered by the graphite does not satisfy the customers' energy demands. These two motivations lead researchers to deepen their investigations about fabricating new anode material for LIBs.

Table 2.4 gives a comparison of the alternative anode materials (Li, C, LTO, Si, Sn, Sb, Al, Mg,) properties (density, capacity, volume changes performed upon cycling and reaction potential with lithium) .

Table 2.4 : Electrochemical properties of some anode materials [26].

Material	**Li**	**C**	**$Li_4Ti_5O_{12}$**	**Si**	**Sn**	**Sb**	**Al**	**Mg**
Density(g/cm^3)	0.53	2.25	3.5	2.33	7.29	6.7	2.7	1.3
Lithiated phase	Li	LiC_6	$Li_7Ti_7O_{12}$	$Li_{4,4}Si$	$Li_{4,4}Sn$	Li_3Sb	LiAl	Li_3Mg
Theorical specific capacity(mAh/g)	3862	372	175	4200	994	660	993	3350
Theorical charge density(mAh/cm^3)	2047	837	613	9786	7246	4422	2681	4355
Volume change (%)	100	12	1	320	260	200	96	100
Potential vs. Li(~V)	0	0.05	1.6	0.4	0.6	0.9	0.3	0.1

In many cases, when the reduction potential of the electrolyte is higher than the lithiation potential of anode materials, the electrolyte decomposes and oxide film covering the electrode surface (named as 'solid- electrolyte interface') forms. This

film polarizes the electrode surface and changes the electrode's lithiation mechanism upon cycling. Therefore, some scientists have proposed to use $Li_4Ti_5O_{12}$ as the anode material since its lithiation potential is higher than the electrolyte's decomposition temperature. But its low theoretical capacity (155 mAh/g) restricts its wide use in commercial applications [27].

Alternatively, silicon and silicon based electrodes are widely studied to replace the state-of-the-art electrode:graphite. Its high abundance on earth, low cost, high gravimetric (3579 mAh/g at room temperature) and volumetric (2400 mAh/cm^3) capacities make them promising candidates for next generation anode materials. However, the low rate performance and the short cycle life of such Si electrodes inhibit their commercialization. The intrinsic low electrical conductivity and the high volumetric expansion (>%300) causing lost of electrical contacts among active particles and particles with the current collector may elucidate the reason of this weak performance [39,40].

Germanium (Ge) is another candidate of next generation anode mateirals. Its high theoretical capacity (1623 mAh g^{-1}), intrinsic electrical conductivity and Li diffusion rate promote its uses in reasearches. However, smilar to Si, Ge shows high volume changes (%300) upon cycling which decreases its cycling stability as well as coulombic efficiencies [41].

Tin (Sn) also has been investigated as an anode material for LIBs. Sn performs high theoritical capacity (990 $mAhg^{-1}$) and undergoes high volume changes (220%) upon lithiation and delithiation reactions [42].

Lloris et. al [23] have classified the lithium reaction's mechanisms of different anode materials (Figure 2.2) in three groups: intercalation, alloying, conversion.

Intercalation occurs when lithiation occurs at low working potentials with a small, flat working voltage plateau. The electrode material should have an open structure to accomodate Li ions. They have longer cyclability as a result of relatively small/no volume change within the structure during Li ions insertion. However, they are limited by their low specific capacities (170-400 mAh/g). The most important intercalation material is graphite: in charging, 1 Li ion settles within the basal plane of the 6 C atoms. This mechanism provide 372 mAh/g capacity to graphite.

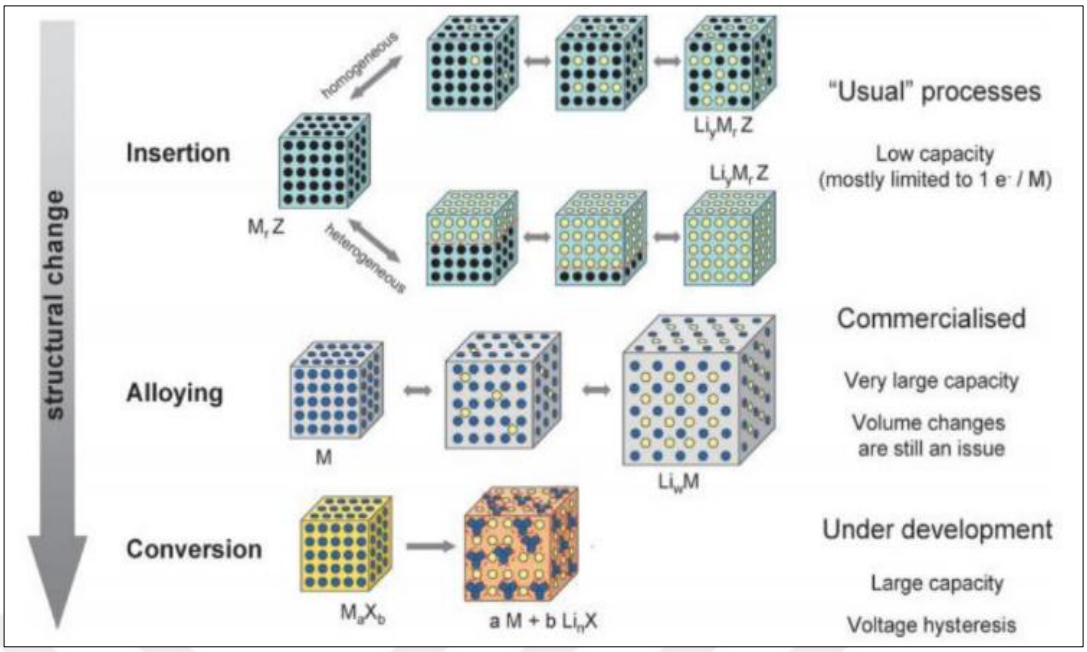

Figure 2.2 : Schematic representing the different reaction mechanism of electrode materials [24].

In alloying, the electrode material performs the highest reversible capacity (800-1800 mAh/g) along with low working potential and relatively good power capabilities. They have higher specific capacities (900 – 3000 mAh/g) as compared to other materials. For this type of reaction, phase diagram becomes very important. Their wide commercialization is hindered due to their low structural stability caused by great size expansions occurred in discharging [43].

In conversion, metal oxide may react with Li reversibly. Therefore, conversion anode materials have attracted great interest. The major advantages of this mechanism is the capability to store more than 1 Li ions per unit compound due to multiple oxidation states of the electrode material. For this reason, conversion type materials are capable of higher reversible capacity (500-1100 mAh/g). However, great size expansion in the the anode causes structural damages, eventually. Thus, often this type of anodes perform poor cyclability. Nano sized transition metal compounds which have the formula M_cX_d (M = 3d transition metal, X = O, S, P, N, etc.) are found to perform better in comparison to others. The electrochemical reaction of the conversion metal oxide compounds with Li is given in Equation 2.1[43] ;

$$M_cX_d + (d \cdot n)Li^+ \leftrightarrow cM + dLi_nX/ \qquad (2.1)$$

where n is the redox number of the anionic compounds X.

2.3.5 Transition metal oxide anode

The transitional metal oxides become remarkable due to their high capacities. However, their low capacity retention, low coulombic efficiency and cycle life restrict their commercialization. In 2002, Poizot et. al [28] have published a paper where they claimed that they increased the energy density as well as the cycle life and the coulombic efficiencies of the electrode materials by nanostructuring. In this sense, in last 20 years several metal oxides have been investigated as a candidates of new anode materials for LIBs. Among them, tin oxide, titanium oxide, iron oxide and ternary ($A_xB_yO_z$) metal oxides are the outstanding anode materials. These metal oxide metarials demostrate many advantages, such as high reversible capacity (2-3 times) in reference to carbon and good stability compared to Si and Sn metalic anodes. Also their wide spread avability and enviromental friendly nature are the other advantages of metal oxide anode materials [29].

Lithiation mechanism of transition metal oxides have been studied by various research groups. Results show that particle size, particle composition, particle structure, and lithiation potential affect this reaction. In the past decades, as stated above, conversion reaction which is a novel mechanism in some metal oxide anode materials has been discovered (Equation 2.2 and Equation 2.3).

When metal oxide materials use as a negative electrode, oxygen reacts with lithium preferentially (see Equation 2.2) and lithium reacts with metal further in discharging as described by Equation 2.3 [30] ;

$$(2y-x)Li + Li_xMO_y \rightarrow yLi_2O + M \quad (2.2)$$

$$xLi + M + e \rightarrow Li_2M \quad (2.3)$$

2.3.5.1 Fe based metal oxide

Iron oxide is one of the most commonly used transitional metal oxides in material science. It has different crystal structures (Fe_3O_4 and Fe_2O_3) that have theoretical capacities varying from 926 to 1005 mAh/g [31].

Recently, scientists have highlighted the promising performance of iron oxides as anode material due to their high theoretical capacities, envionmentally benign behaviors and high abundance on earth. Table 2.5 shows the properties of the iron

oxide powders that have been fabricated differently and their electrochemical performances when used as anode material in lithium ion batteries.

Table 2.5 : Electrochemical properties of some iron oxide powders that are used as anodes for LIBs.

Morphology	Particle size (nm)	Current rate (mA /g)	Reversible Capacity (mAh/g)
Fe_3O_4 nanowires[31]	nanowires, 20−50 nm diam; several micrometers length	0.1C	915
Fe_3O_4 hollow spheres[32]	500 nm diam; 150 nm thickness	100	1120
Fe_2O_3 nanoflakes[33]	700 nm film thickness	65	810
Fe_2O_3 nanorods[34]	40 nm diam, 400 nm length	201	908
spindle-like porous Fe_2O_3[35]	spindle length 0.8 μm, width 0.4 μm; <20 nm	200	940
Fe_2O_3 micrometer size[36]	5 μm size	100	700
Fe_2O_3 nanosize[35]	∼25 nm size	100	1000

2.3.5.2 Ti based metal oxide

Rather than titanium, titanium oxides are widely used in fotocatalyser, semi conductor, sensors, and anode materials in Li-ion batteries. TiO_2 may have different crystal structure revealing different physical properties [37].

Although the theoretical capacity is very low compared to the graphite (336 mAh/g for anatase) its high lithiation potential (0.7 V vs. Li/Li^+) prevents the SEI formation, leading high cycle retention upon cycling. Plus, its high electronic and ionic conductivities make it a great candidate for metal oxide anode materials of LIBs.

Table 2.6 summarizes the properties of the TiO_2 powders that have been fabricated by different methods and their electrochemical performances when used as anodes in LIBs. TiO_2 materials have attracted great attentions due to their unique properties

such as high power densities, safety and non-toxicity. They store 1 lithium per mol TiO_2 according to following Equation 2.4[37]:

$$TiO_2 + x(Li^+ + e^-) \leftrightarrows Li_xTiO_2 \quad \text{with } x = 1 \tag{2.4}$$

Table 2.6 : Electrochemical properties of TiO_2 anode materials.

Structure	Morphology	Particle size (nm)	Current rate (mA /g)	Reversible Capacity (mAh/g)
Anatase	TiO_2 nanoparticles[38]	6	0.05C	165
	mesoporous TiO_2[39]		0.05C	100
	TiO_2 nanosheets[39]	18.8	0.05C	118
	amorphous TiO_2[40]	2−3	0.2C	335
	spherical[41]	9−11	0.2C	270
	nanofibers[42]	18	0.45C	144
	nanoporous calcined (at 400 °C)[43]	9.5	0.2C	229
Rutile	'needle-shaped' Morphology [44]	10 nm diam., 30−40 nm length	0.05C	205
	commercial nanoparticles[44]	15 nm	50	264
	'rod-shaped' particles[45]	200 nm long, 10 nm diam.	30	160
	bulk[45]	1 μm	30	10
	spherical particles[46]	size 1.5−3 μm, 20 nm nanorods	0.033C	200

3. PRODUCTION OF METAL OXIDE POWDERS

In literature, several methods such as microwave synthesis, spray pyrolysis, combustion synthesis, sol-gel and hydrothermal have been used to produce metal oxide powders. Table 3.1 gives a comparison of those methods.

Table 3.1 : Some metal oxide production method.

Method	Advantages	Disadvantages	Ref.
Microvawe	Easy to produce Less amount of solvent is required Enviromentally friendly	Low amount of production	[47]
Combustion	Simple, Fast, High rate of heating and cooling,	Not economical	[48]
Hydrothermal	Morphological controlled synthesis, High purity, narrow size disturibution	Expensive price of autoclave, not possible to in-situ analysis	[49]
Spray Pyrolyse	Various composition and morphology, Produce from metal salts	Long processing time	[50]
Sol-Gel	Low temperature, Enviromental friendly, Low invesment cost	Expensive precursor, air sensitive	[51]

Unlike to literature, in this thesis, the recovery of metals from a product to fabricate metal oxide powders have been studied. In this sense, extractive metallurgy principles have been used during the production.

There has been no published work on the acidic leaching of ferro titanium alloys, instead acidic leaching of ilmenite has been reported [52]. Considering the experience from ilmenite leaching, and extractive metallurgy principles, first in literature, a new process is designed to recover both titanium and iron ions from ferrotitainum alloys to fabricate two products:iron rich- and titanium rich- oxide powders.

3.1 Metal Oxide Fabrication from Ilmenite

In literature, Ti ores are classified in five groups: rutile (TiO_2), perovskite ($CaO{\cdot}TiO_2$), ilmenite ($FeO{\cdot}TiO_2$), pyrochlore $(Na,Ca,\ldots)(Nb,Ti)_2O_6(F,OH)$, and sphene $CaTiSiO_4{\cdot}(O,OH,F)$. Among these raw materials, ilmenite is the most important and the most common titanium minerals with a known total word resources $\sim 2\times10^{12}$ kg. Ilmenite is the major sources of TiO_2 pigment(Fig.3.1). The World production of ilmenite and rutile are 10 million and 700 thousand, respectively. Approximately 95% of the world's production of titanium mineral feedstock is consumed in the production of titanium dioxide (TiO_2), an intensely white colour pigment used as a base in coatings, plastics and paper production [53].

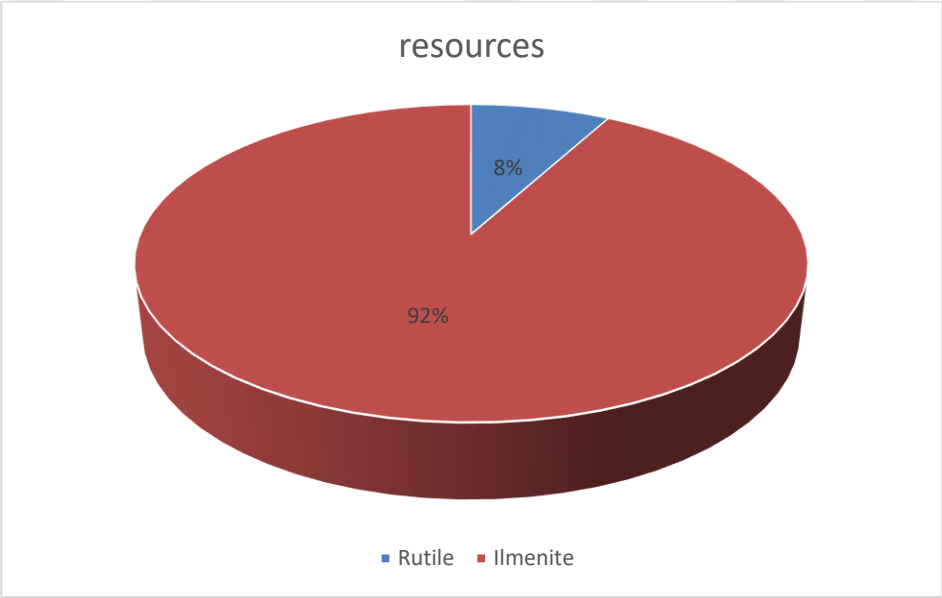

Figure 3.1 : World resources of rutile vs ilmenite [53].

3.1.1 Basic leaching

So far, potassium hydroxide [54], sodium hydroxide [55], ammonium hydroxide [56] have been used in basic leaching process.

Table 3.1 summarizes the studies and their optimum conditions to leach ilmenite material.

It is noteworthy to claim that none of these studies recover iron from the leachate and none of them analyses the use of titanium oxide as anode materials for lithium ion batteries. The latter highlights the uniqueness of this thesis.

Table 3.1 : Some example of ilmenite alkali leaching.

Leach agent	Acid concentration	Solid/Liquid	Temperature(°C)	Time	Ti leach	Fe leach	Ref.
KOH	80 wt.%	1:7	220	2h	85wt.%	-	[54]
NaOH	2.5M	1:10	120	14h	42 wt.%	-	[55]
NaOH	0.3M	-	220	80min	30wt%	-	[55]
NaOH	10M	1:4	220	4h	99 wt%	-	[57]
NH4OH	4M	1:1.5	150	2h	99.8wt%	-	[56]

3.1.2 Acidic leaching

In literature, ilmenite has been leached out by using different type of acids (HCl [58] H_2SO_4[59], H_3PO_4 [60]). Some researchers have investigated the parameters affecting the leaching efficiency and found that leaching time, temperature, acid type, acid concentration are mainly responsible for the efficiency.

Jia et al [61] have investigated ilmenite leaching efficiency and found that they have achieved 85% riched TiO_2 powders when ilmenite has been leached out by sulfuric acid. They have argued that when the reaction temperature increases, the dissolution of iron from ilmenite enhances. Moreover, high sulfric acid concentration results in agglomeration of hydrolysate particles and this particles adsorp onto the unreacted particles, thus retarding the ilmenite leaching process. The optimium conditions of the enrichment ilmenite have been reported as 40 wt.% acid concentration, acid/ore mass ratio 2:1, reaction temperature 150 °C and reaction time 3 h. Li et. al [62] have also investigated the effect of the sulfuric acid concentration, pre-heating of the raw material, acid molar volume ratio and reaction time on the decomposition efficiency of ilmenite (based on the dissolved amount of metal ions in the solution). They have found that the optimal H_2SO_4 concentration is 0.32 mol/L and the decomposition of ilmenite increases at longer duration then gets stabilized after 120 min. The maximum efficiency is found as follows: 0.32 mol acid concentration, 120 min., 160 °C and 13.5 mol/L H_2SO_4 solution. The decomposition rate increase with an increase in the initial preheating temperature and reached 95% at 160 °C.

Other than the above mentioned studies, in literature there are also remarkable researches that focus on the decomposition of ilmenite in acidic solution. Table 3.2 summarizes these studies with their optimum parameters[61-66].

Table 3.2 : Some example of ilmenite acid leaching.

Acid	Acid concentration	Solid/Liquid	Temperature(°C)	Time	Ti leach	Fe leach	Ref.
H_2SO_4	40 wt.%	1:20	150	3h	84 wt.%	-	[61]
H_2SO_4	15 mol/L	-	90	2h	95.21 wt.%	-	[62]
H_2SO_4	%20	1:100	100	50min	85wt.%	90wt.%	[63]
HCl	5M	3.3%w/w	70	4h	94wt%	93 wt%	[64]
HF	6.4M	1:20	Boling point	5h	81 wt%	26wt%	[65]
HCl	20wt%	1:50	105	6	8wt%	85%	[66]

3.1.3 Metal oxide fabrication from ferrotitanium

Once the composition's effect on material properties has been discovered, elements have been used as an alloying additive in steel industry. Some alloys are added into the molten steel to strenghten. Herein, pure elements may be used as additives but their high price and low stability at high temperatures make them impractical. Instead, use of ferroalloys as additives becomes very attractive since they are highly stable at high temperatures and relatively cheaper in price [83,84].

Ferroalloys are made of one or more alloying elements (except carbon) with iron. They contain iron, alloying elements and low amounts of impurities (phosporous, sulfur and nonferrous metal). They are primarily used in steel industry (%85-90), and a small amount is utilized in non-ferrous industry as well. Ferroalloys can be divided into bulk ferroalloys and noble ferroalloys (also called special or specialty ferroalloys). Bulk ferroalloys are produced in large quantities and include ferrochromium. Noble ferroalloys are produced in smaller quantities and typically include ferroboron, ferromolybdenum, ferronickel, ferroniobium, ferrophosphorus, ferrotitanium, ferrotungsten, and ferrovanadium, among others [83].

Ferrotitainum is a noble ferroalloy which primarily consists of iron and titanium. Also, it contains aluminum, manganese and some impurities elements like silicon, carbon, sulfur and phosphorous. Ferrotitainum have titanium by range of 20-75% (wt). The phases in ferro titanium alloys are mostly found to be: FeTi, Fe_2Ti and $FeO{\cdot}TiO_2$ phases and also α-Ti and β-Ti. Although β-Ti is not thermodynamically stable at room temperature, the fabrication process of this commercial product may

lead to the formation of non-equilibrium phases [83,85]. Moreover, 'unlimited mutual solubility' is noted in their liquid phases [67]. But in the solid phase, they form intermetallic compounds such as TiFe and $TiFe_2$ (see Fig.3.2).

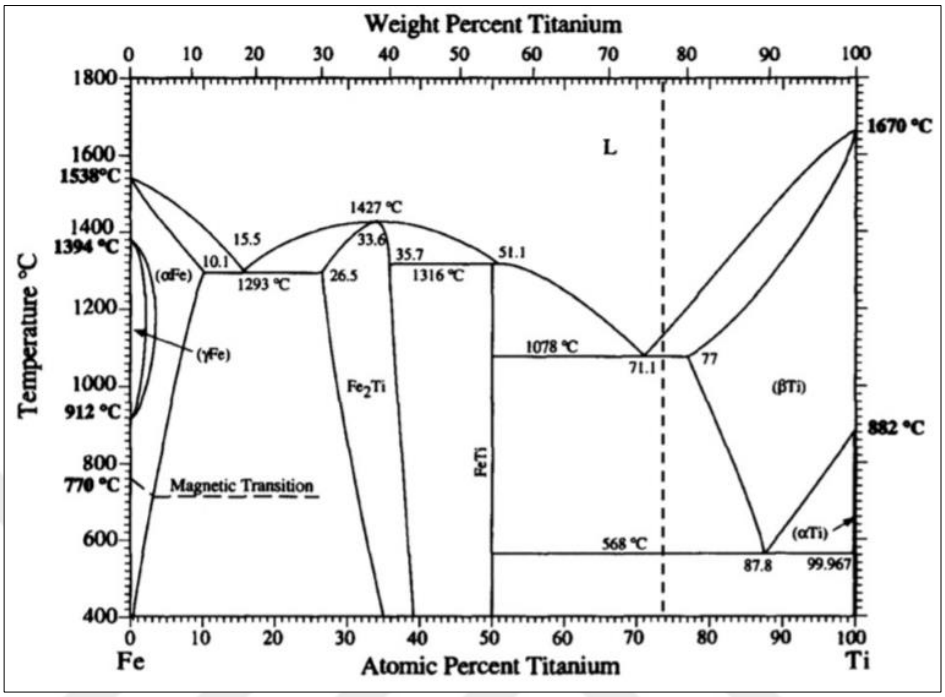

Figure 3.2 : Fe-Ti phase diagram. [67].

As stated previously, many research groups have been working to extract TiO_2 of different shapes and sizes from ilmenite. But no published paper/manuscript/report has been found about the fabrication of metal oxide powders through ferrotitanium alloys.

This thesis represents a new methodology to fabricate iron oxide and titanium oxide powders by using ferrotitainum alloys as the raw material. Through the acidic leaching of ferrotitanium alloys nanometer sized pure titanium oxide powders have been achieved along with iron oxide powders from the waste solution of titanium oxide.

Characterization results show that ferrotitanium and ilmenite have similar elemental compositions although their structures differ from each other. Ilmenite has a $FeO{\cdot}TiO_2$ phase more than ferrotitainum because, during the production of ferrotitainum alloys oxide particles are formed, then chemically reduced to form Fe-Ti intermetallics. Other than Fe and Ti, ferrotitainum has additional impurities such as Al, Mg, Si, Mn etc...(Table 3.3).

However, the fact that less amount of impurity elements present in ferrotitainum alloy (in comparison to ilmenite), highly pure TiO_2 is proceed very successfully.

Table 3.3 : The chemical composition of ferrotitainum and ilmenite [67].

Alloy grades	Ti	Si max	Al max	Mn max	P max	S max	C max
A	64-76	0.24	0.51	0.50	0.050	0.050	0.15
B	64-76	0.24	5.0	1.5	0.050	0.050	0.20
C	39-44	5.0	8.1	1.6	0.10	0.050	0.15
D	16-24	5.1	8.1	1.6	0.10	0.060	0.15
Ilmenite	26.5	0.4	0.7				

3.1.4 Taguchi methods

Taguchi's experimental design allows to optimize the outcome of a more economical way with fewer experiments [68]. This methodology has taken the design of experiments from the exclusive world of the statistician and brought it more fully into the world of manufacturing. Taguchi introduces his approach, using experimental design for [69]:

- designing processes so as to be independent to environmental conditions;
- designing and developing processes so as to be robust to component variation;
- minimizing variation around a desired value.

Taguchi argues that an engineering optimization can take place in system, parameter and tolerance design. The parameter design (selection of parameters and their levels) is done to maximize the quality and the efficiency of the product and/or process. The classic 'parameter design' developed by Fisher has a complex structure. Especially, when the number of parameters is increased, too many experiments are needed. Unlike the classical method, Taguchi method uses a special design of orthogonal arrays. The benefit of this method is that it allows to examine the effect of all parameters and interactions if needed by performing fewer experiments.

The 'loss function' in Taguchi is defined based on the difference between the determined and the experimental values. Taguchi proposes the use of the loss function to evaluate the performance characteristic aberrating from the requested value. The value of the loss function is further converted to a signal-to-noise (S/N)

ratio. S/N ratio is examined in three categories, small-is-better, nominal-is-the best and higher-is-better. Furthermore, a statistical analysis of variance(ANOVA) is executed to obtain which process parameters are statistically important. With the ANOVA and S/N analyses, the optimal combination of the parameters can be predicted. Lastly, a verification experiment is carried out to verify the optimal process parameters [70].

4. EXPERIMENTAL PROCESS

4.1 Grinding

Within the scope of the thesis, first powders are cracked with a hammer then ground (Siebtechnik) to decrease the particle size.

4.2 Sulphuric Acid Leaching

During the leaching, sulfuric acid (Merck, 96%) have been used as a starting material. Then, oxalic acid (Sigma, 98%), sodium hydroxide (pellet form, Merck %97) and ammonia (Tekkim ,525 extra pure) have been used in the powder production.

Sulphuric acid leaching has been done following Taguchi experimental approach. With the help of 9 experiments, 18 different oxide powders have been produced. With selected parameters and levels Table 4.1. show s the L9 experimental design.

Table 4.1 : L9 experimental design with selected praameters and their levels.

Experimental No	Molar of acid	Temperature	Solid/liquid Ratio	Leaching time
1	1	80	1/50	1
2	1	100	1/100	3
3	1	120	1/25	6
4	0.5	80	1/100	6
5	0.5	100	1/25	1
6	0.5	120	1/50	3
7	3	80	1/25	3
8	3	100	1/50	6
9	3	120	1/100	1

4.2.1 Fabrication of metal oxides anodes

The flow chart in Figure 4.1 has been followed during experimental studies.

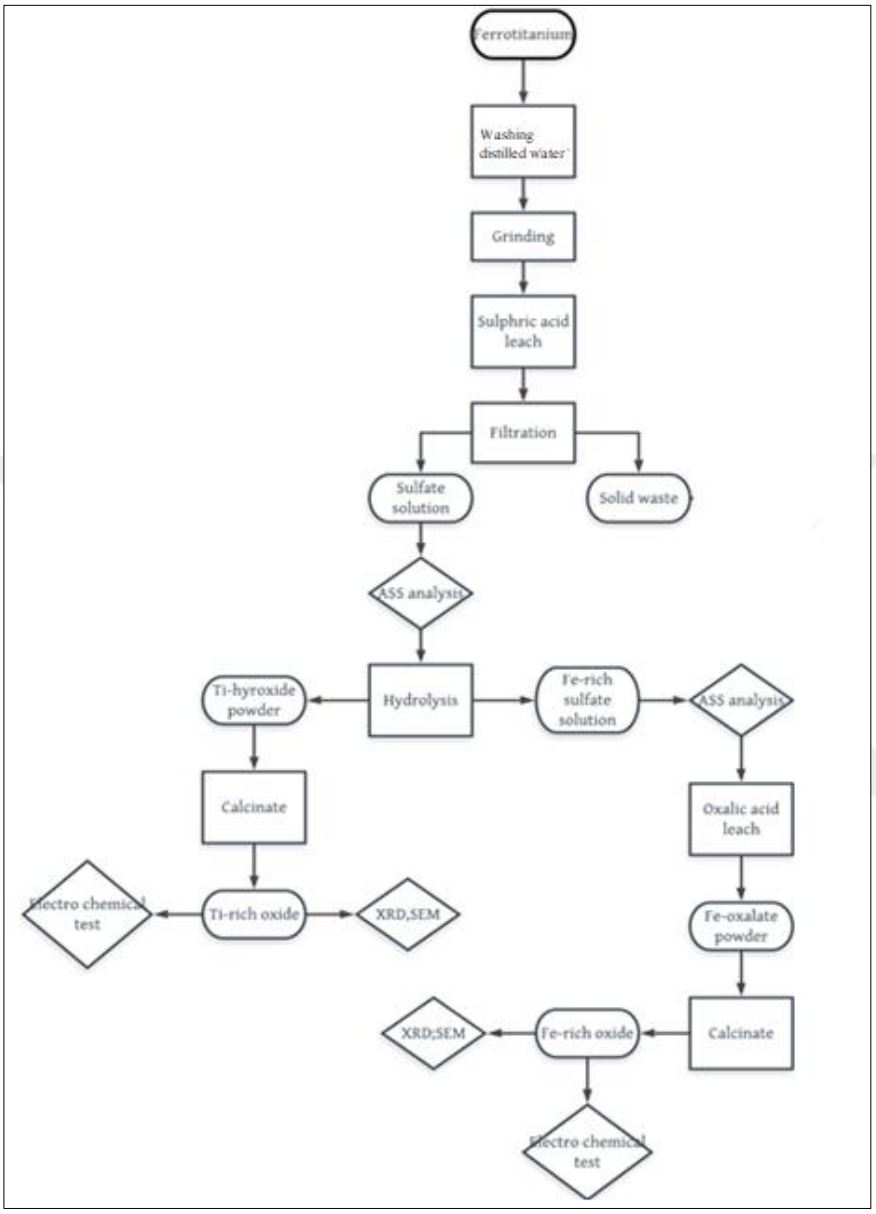

Figure 4.1 : The flow chart of ferrotitanium experimental process.

All experiments are carried out in an oil bath using a 250 ml flask with a magnetic stirrer. 2 ml of ferrotitanium powders have been used as the precursor material in each experiment. First, ferrotitanium powder is washed with distilled water at 60 ^{o}C to remove organic salts. Then, desired acid concentration and solid/liquid ratio have been prepared. The temperature has been adjusted for each experiment and finally ferrotitainum powders have been added slowly into the acid solution. For each experiment the solution has been continuously rotated with a magnetic stirrer at 400

rpm. Once the leaching has been done, filtration has been applied to separate liquid and solid (waste) particles. The liquid (sulfate) solution has been transferred into a beaker and two times of its volume has ben poured down to dilute it. Then, the diluted solution has been heated up until it gets boiled. While it has been boiling, the pH of the electrolyte has been fixed to 1 with sodium hydroxide (5M solution).

After the colour of hydrolyzed solution turn creamy white, Ti-rich powders have been precipitated at the bottom of the beaker. Filtration has been applied to separate the titanium rich powders from iron sulfate rich solution. Once the precipitated titanium rich powders have been cleansed with distilled water and ethanol, they are placed in an oven for over night at 70 ^{o}C. After drying, heat tratment has been applied at 600 ^{o}C for 240 minutes (5^{o}C/min).

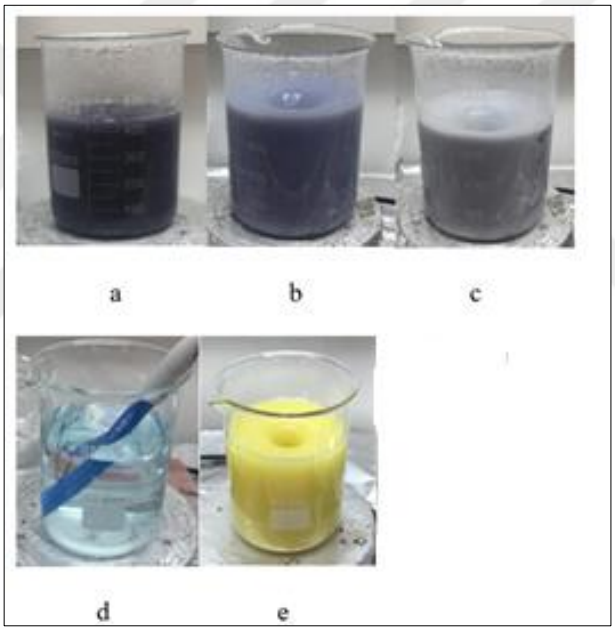

Figure 4.2 : a) Sulfate solution, b) 3 hours hydrolysis, c) 5 hours hydrolysis, d) Fe-rich sulfate solution, e) Oxalate leach.

40 ml oxalic acid has been added into the each remained iron sulfate solution and the pH of the solution has been adjusted to 3 with ammonia. This step causes a change of solution color from blue to dark yellow (Fig.4.2). Then, yellow ferrous oxalate powders have been precipitated at the bottom of the beaker and filtrated. The powders have been cleansed with distilled water, and ethanol then dried at 70 C^{o} over night. Finally, the powders have been calcinated at 500 C^{o} for 120 minute to produce Fe-rich oxide powders.

4.3 Slury Preparation

For each slurry preparation the oxide powders (Ti-rich or Fe-rich powders) have been mixed with carbon black conductive agent (Alfa Aesar, %97), and PVDF (solved in NMP) (Alfa Aeser %98) with 8/1/1 ratio in Thinky ARE250 to get a semi-viscous slurry.

4.4 Lamination

The prepared slurry has been spread on the 15 μm thick copper foil (99.98% purity) by doctor blade technique. The thickness of the lamination has been adjusted to 50 μm (Fig. 4.3). Then, the coating has been replaced into a vacuumed furnace and dried at 70 ^{o}C for 720 minutes. And finally, it has been rolled twice to further decrease the film thickness.

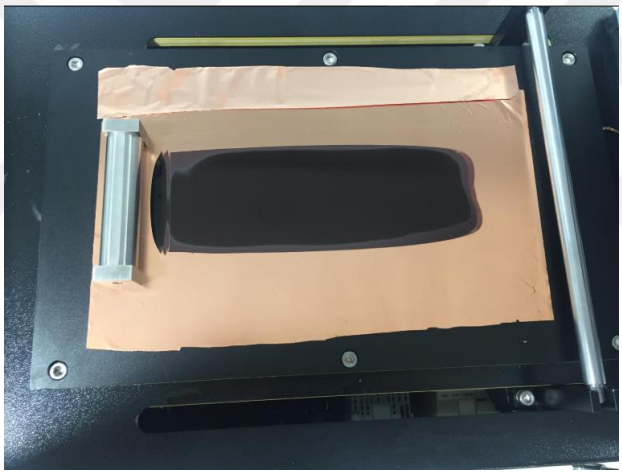

Figure 4.3 : Lamination on Cu foil.

4.5 Battery Assemble

In order to make electrochemical tests, CR2032 standard coin cells have been assembled in the glove box (MBRAUN, Labmaster) where oxygen and humidity levels are always smaller than 0.1 ppm. The cell has been created by stacking a separator (Celgrad 2400) between the working electrode (metal oxide anode) and the counter electrode (Li foil), followed by the injection of liquid electrolyte (1M $LiPF_6$, EC:DMC).

4.6 Characterization

4.6.1 Wet chemical analysis

The amount of iron ions after sulfuric acid leaching and hydrolysis have been detected by atomic absorption spectroscopy (Shimadzu AA6200).

4.6.2 Compositional, morphological and structural characterization of powder

XRF method (Hitachi X-MET8000 XRF) has been used to find the composition of the initial ferrotitanium powder. The fabricated metal oxide powders have been characterized by secondary electron microscopy (Zeiss Gemini 500). The elemental mapping of the powders has been done by EDS analysis (Bruker). The structure of the powders has been examined by X-ray Diffraction Method (Rigaku Desktop,) between 10-90˚ with 5˚/minute scan rate. Cu Kα radiation has been used in all experiments.

4.6.3 Electrochemical chacterization

The electrochemical performances of the cells have been measured by MTI BST8-WA battery analyzer. The electrodes have been cycled between 0.001-3 V at 50mA/g current rate.

To analyze the lithiation mechanism of the electrodes, cycling voltammetry has been performed between 0.001-3 V with 0.5 mV/s scan rate, during the first 3 cycles of each electrode. A potentiostat (Gamry Interface 1000E) has been used for the characterization.

5. RESULTS AND DISCUSSION

5.1 Grinding

Ferrotitainum chunk have been crushed by a hammer then ground with a mill (Siebtechnik) (see Fig.5.1). The SEM image shows that the powders have an irregular morphology and their avarege particle size is about 10 μm(Figure 5.2).

Figure 5.1 : Siebtechnik mill.

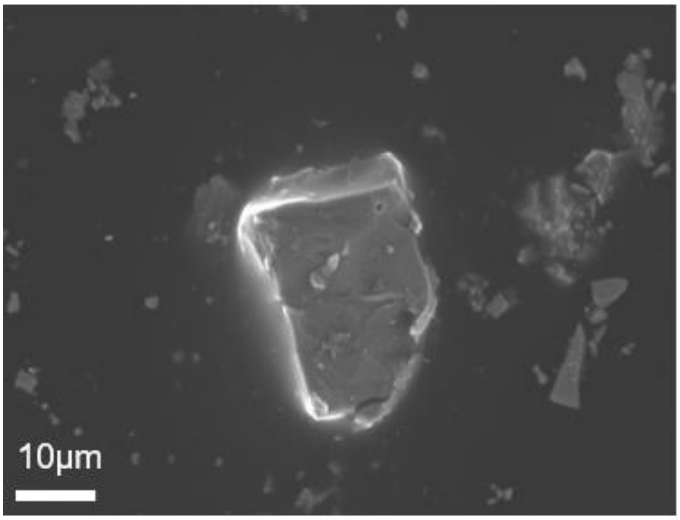

Figure 5.2 : SEM image of ferrotitanium particle.

XRD analyses(figure 5.3) show that, ferrotitanium consist of Ti_2O_3, TiO_2, Fe_2TiO_4, and Fe_2Ti phases.

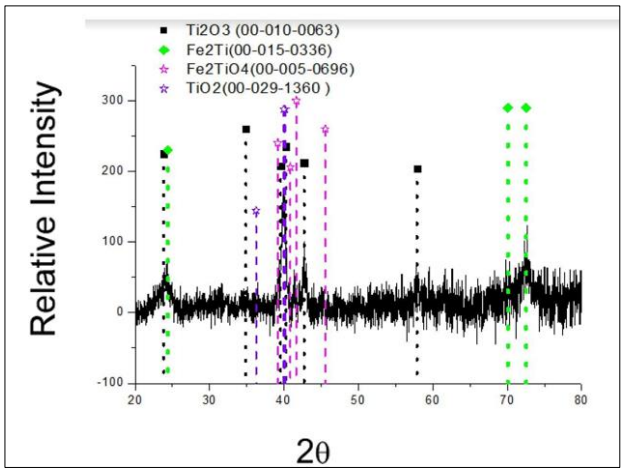

Figure 5.3 : XRD analyses of ferrotitanium.

XRF analyses show that (Table 5.1), Ti and Fe are the major elements of ferrotitanium. Also, there are less than %1 percent impurity metals.

Table 5.1 : XRF analyses of ferrotitanium.

Elements	Percent
Ti	%70
Fe	%23
Al	%1
Mn	%0.3
Mo	%0.3
Cr	%0.2
Va	%0.1
Ni	%0.1

5.2 Sulfuric Acid Leaching

The ground ferro titanium alloys have been leached out by sulfuric acid following the Taguchi experimental design. Molar acid ratio, electrolyte temperature, solid/liquid ratio, leaching duration have been chosen as process parameters. Table 5.2. shows the parameters and their levels used in the experiments.

Li et al [63] have studied the sulfuric acid leaching of ilmenite and found that acid leaching is unselective and both titanium and iron are dissolved following their stochiometric ratio in the precursor material, under their experimental conditions (%15 H_2SO_4 solution concentration, 100^0C, 4h). Herein, the possible differences in the leaching efficiencies of titanium and iron are believed to be related to their different reaction kinetic.

Table 5.2 : Taguchi experimental design.

Parameters	Molar acid ratio(M)	Electrolyte Temperature(^{0}C)	Solid/liquid ratio(mL/mL)	Leaching duration(h)
Level 1	1	80	1/50	1
Level 2	0.5	100	1/100	3
Level 3	3	120	1/25	6

In this thesis, first in literature, the metal ion recovery efficiency through ferrotitanium alloy is maximized by Taguchi and parameters' effects on the efficiency are discussed based on ANOVA method. Control experiments have been conducted for titanium oxide and iron oxide powders, separately. For each case, the expected efficiencies agree with the Taguchi's control experiments results.

Knowing that at 14M sulfuric acid solution, at 200^{0}C, solid sulfate particles are precipitated ($TiOSO_4$ (s) and $FeSO_4$ (s)) at the bottom of the flaks (Eq 5.1), the levels of parameters for Taguchi design are selected to get stable titanium ions and iron ions (as well as aluminum ions) in the sulfate solution (Equation 5.2-5.5) [62];

$$FeTiO_3(s)+2H_2SO_4(aq)\rightarrow TiOSO_4\ (s)+FeSO_4\ (s)+2H_2O\ (l) \quad (5.1)$$

$$FeTiO_3(s)+4H^+\rightarrow TiO^{2+}(aq)+Fe^{2+}(aq)+2H_2O\ (l) \quad (5.2)$$

$$Fe_2O_3(s) + 6H^+\ (aq) \rightarrow 2\ Fe^{2+}(aq) +3H_2O\ (l) \quad (5.3)$$

$$TiO_2(s) + 4H^+\ (aq) \rightarrow Ti^{2+}\ (aq) + 2H_2O\ (l) \quad (5.4)$$

$$Al_2O_3(s) + 6\ H^+\ (aq) \rightarrow 2\ Al^{3+}\ (aq) + 3H_2O\ (l) \quad (5.5)$$

Table 5.3 : Taguchi experimental design with S/N ratio.

Run No	Molar of acid(A)	Temperature (B)	Solid/ Liquid Ratio (C)	Leaching Time (D)	TiO_2 weight (g)	S/N ratio	Fe ions from AAS-1 (g/l)	S/N ratio
1	1	80	1/50	1	1.40	2.92	1.65	4.34
2	1	100	1/100	3	2.70	2.92	1.76	4.91
3	1	120	1/25	6	1.40	8.62	1.58	3.97
4	0.5	80	1/100	6	0.30	2.92	1.74	4.81
5	0.5	100	1/25	1	0.60	-10.45	1.45	3.2
6	0.5	120	1/50	3	0.80	-4.43	1.83	5.24
7	3	80	1/25	3	2.25	-1.93	1.60	4.08
8	3	100	1/50	6	4.00	7.04	1.85	5.34
9	3	120	1/100	1	7.40	12.04	1.88	5.48

5.3 Titanium Oxide Powder's Production and Characterizations

5.3.1. Taguchi experimental design analysis for TiO_2 formation

Powder formation yield is calculated based on the weight of TiO_2 powders after calcination step. Table 5.3 shows the calculated S/N ratios considering Taguchi's "larger is better" approach. Equation 5.6 has been used to calculate S/N values. Where n is the number of observations and y is the observed data. The effects of parameters are calculated by averaging the S/N ratio for each level.

$$S/N=-10*\log(1/n\Sigma(\ 1/y_i\text{^}2)) \qquad (5.6)$$

Table 5.2 shows the parameters and their levels used in the Taguchi design. Herein molar acid ratio is chosen as a parameter because Li et al. have revealed that, the decomposition rate of ferrotitanium is increased with an increase in sulfuric acid concentration. The increased interactions of solid particles' with H^+, SO_4^{2-} may elucidate this observation [71].

Leaching time and solid/liquid ratio are also selected as effective process parameters for titanium oxide fabrication because in prolonged duration partial evaporation of the solution (changing the solid/liquid ratio) occurs and homogeneous ionic distribution in the flask gets disturbed. Further increase in the process duration causes a decrease in titanium oxide formation. It is thought that sulfuric acid etching effect prevails in the solution and titanium hydroxide particles forming in longer duration is re-dissolved.

Finally, temperature is also investigated as an effective process parameter.There are some thresholds of temperature: 25-100^{0}C temperature increases leaching efficiency on a limited scale. Further increase in temperature (160-170^{0}C), the surface reaction rate of ferrotitanium alloy as well as its decomposition rate increases. When the solution temperate gets too high the solubility of Ti-sulfate products decreases, resulting lower titanium oxide efficiencies [63].

To further discuss the parameters' effects on titanium oxide formation efficiency (Figure 5.4), ANOVA analysis has been conducted (Table 5.4). For this study, leaching temperature is found to be least effective parameter compared to others. This could be related to the fast leaching kinetics of titanium and iron in the defined experimental conditions.

Seeing that temperature is the least effective parameters, a revised ANOVA analysis has been accomplished (Table 5.5). Herein, the temperature's effect is pooled into error function.

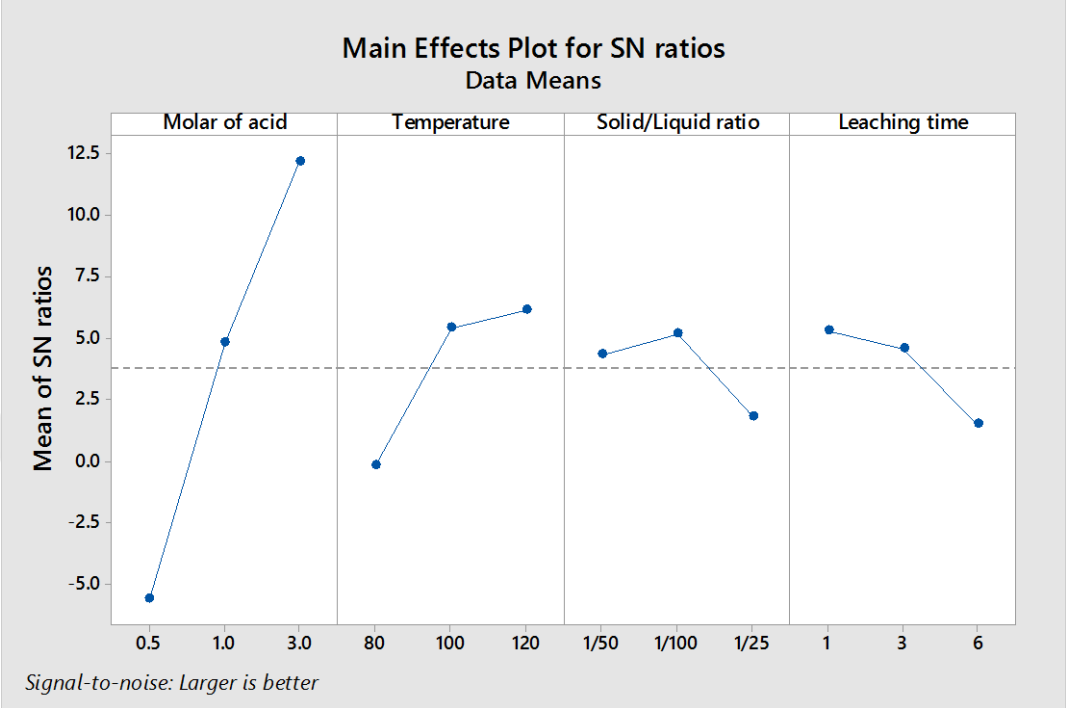

Figure 5.4 : Main effect plot for S/N rations of TiO_2 crystallization yield.

The effects of parameters are calculated by averaging the S/N ratio for each level. Since the experimental design is orthogonal, it enables one to separate the effect of each parameter at different levels (Equation 5.7) [70].

$$A1 = \frac{Exp\ No.1 + Exp\ No.2 + Exp\ No.3}{3} \tag{5.7}$$

Table 5.4 : ANOVA analysis for titanium oxide formation.

Parameter	Degree of freedom	Sum of Square	Mean of Sq
Molarity	2	172.7058	86.35
Time	2	83.09168	41.54
Solid/Liquid	2	78.67519	39.33
Temp.	2	50.09937	25.04
Total	8		

The ANOVA analysis results show that the highest titanium oxide powder formation is achieved when ferro titanium is leached by a 3M sulfuric acid solution (A3) at 120^{o}C (B3), with 1/100 solid/liquid ratio (C2) in 1 hour (D1) (Figure 5.3).

Table 5.5 : Revised ANOVA analysis for titanium oxide formation.

Parameter	Degree of freedom	Sum of Square	Mean of Sq	F value	Contribution
Molarity	2	172.71	86.35	3.44	31.88
Time	2	83.10	41.54	1.65	8.5
Solid/Liquid	2	78.68	39.33	1.57	7.43
Error	2	50.10	25.04		
Total	8				

The maximum weight of titanium oxide that can be fabricated from ferro titanium alloy is calculated following the equation (5.8).

$$u = \frac{T}{n} + \left(\frac{A3}{r} - \frac{T}{n}\right) + \left(\frac{B3}{r} - \frac{T}{n}\right) + \left(\frac{C2}{r} - \frac{T}{n}\right) + \left(\frac{D1}{r} - \frac{T}{n}\right) \quad (5.8)$$

u represents optimum value, T denotes the level totals of each parameters in S/N ratios, n the number experiments (9) and r is the number of replications for each parameter (3) in L_9 (3^4). A3, B3, C2 and D1 are selected to be the maximum levels for parameters in order to get maximum titanium oxide formation. The estimated amount of titanium oxide produced from ferrotitanium alloy (2ml:8.50g) is found to be 8.60 g. The sample 9 in Taguchi (A3 B3 C2 D1) has the same parameters to get the maximum titanium oxide formation. The result shows that 7.40 g titanium oxide is fabricated experimentally under these experimental conditions. The results substantiate that theory gives good agreement with experimental results.

5.3.2. Structural, compositional and morphological characterizations

The phase purity and crystallinity of the Ti oxide powders are characterized by using XRD method (Figure 5.5). Diffraction peaks are well matched with those of the anatase structure (JCPDS 21-1272) with lattice constants a = b = 3.7852 Å and c = 9.5139 Å [72]. The (200) and (004) reflections represent a and c axis of the structure, respectively. Polleux et. al have claimed that equal intensity of (200) and (004)

promotes anisotropic growth of particles leading into a spherical particles formation [73].

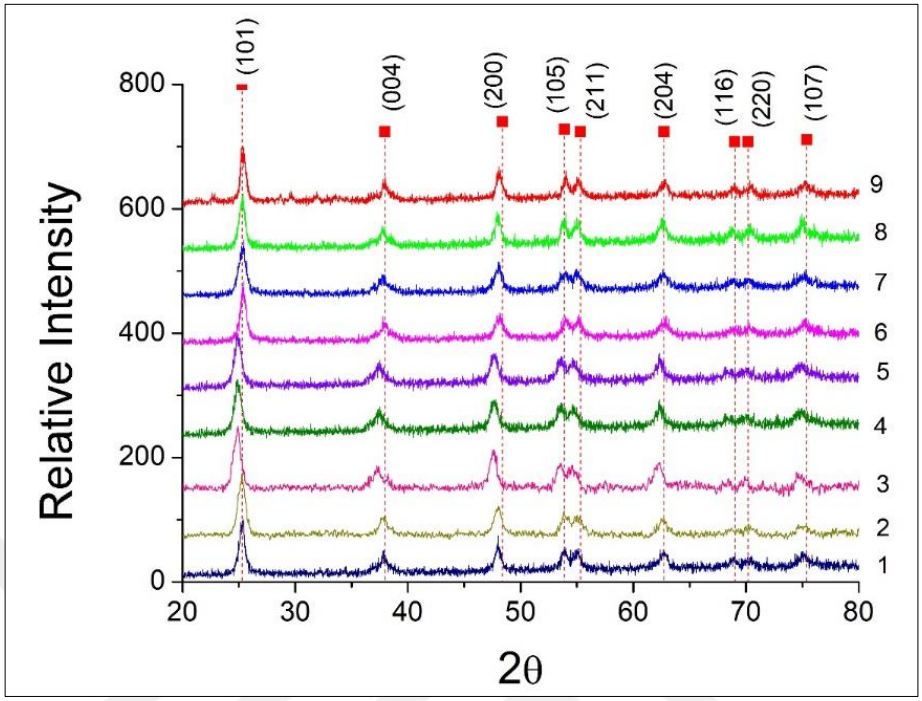

Figure 5.5 : XRD analysis of titanium oxide samples.

EDS analysis has been conducted and results are given in Table 5.6 for all samples. Results reveal that all samples contain different amounts of Ti, Fe, Al, S and Na atoms. Based on these results, it is seen that during the hydrolysis process, Ti and O elements are efficiently extracted from the sulfate solution. The atomic ratios between Ti and O support the stochiometry of TiO_2 structure. Table 5.6 demonstrates that titanium oxide powder contains a very limited amount of Al and Fe atoms compared to the stochiometry of the parent raw material (see XRF results of ferrotitanium alloy). The fact that at low pH values (<3), Fe^{+3} and Al^{+3} ions can not precipitate [62], hydrolysis experimental conditions (ph:1) are selective in order to restrict the co-precipitation of impurities with titanium oxide particles. The trace amount of metal ions present in the TiO_2 powders are believed to improve the electrochemical performance of the metal oxide powders, as suggested by Borghols et al [40].

The SEM images of the hydrolyzed Ti oxide powders after calcination are given in Figure 5.6. The sulfuric acid leaching reactions of different titanum containing compounds are given in Equations (5.1-5.5).

Table 5.6 : EDS analysis of titanium oxide powders (C atom. at.%).

Sample	Ti	O	Fe	Al	S	Na
1	31.62	67.14	0.14	0.35	0.39	0.37
2	39.17	59.63	0.02	0.42	0.55	0.22
3	26.49	71.21	0.03	0.38	0.76	1.09
4	35.35	62.63	0	0.54	0.98	0.50
5	26.97	64.92	1.19	0	6.12	0.80
6	31.27	67.65	0.06	0.01	1.02	0
7	31.33	68.08	0.07	0.09	0.33	0.10
8	27.17	71.84	0.02	0.04	0.58	0.35
9	27.30	71.60	0.05	0.07	0.08	0.20

Once titanium is present as ions in the acidic solution, the hydrolysis occurs following Equation (5.9) [63].

$$TiO_2^{+}(aq) + 2H_2O\ (l) \rightarrow H_2TiO\ (s)\downarrow + 2H^{+}(g) \qquad (5.9)$$

Previous studies about TiO_2 fabrication reveals that in most of the cases spherical shaped TiO_2 powdes are fabricated after sulfuric acid leaching, hydrolysis and calcination [62-66]. SEM images of samples 1, 2, 4, 5, 6, and 7 also demonstrate that they have spherical form similar to the literature [62-66]. The diameters of spherical structures vary between 400 nm and 1 micrometer.

Wang et. al [74] have claimed that the spherical morphology of TiO_2 powders are mostly related to the hydrolysis conditions. They have stated that the sulfuric acid concentration and amount of titanium ions present in the leach solution are the significant parameters which mainly control the hydrolysis of titanium [74]. Tian et. al [75] have defined H_2SO_4/ TiO_2 (mass/mass) ratio and expressed that in hydrolysis higher ratio inhibits the hydrolysis of TiO_2 and decreases the rate of initial particles nucleation. The latter results in larger particles formation since the growth of initially nucleated particles is promoted [75]. On the contrary, at lower H_2SO_4/ TiO_2 (mass/mass) ratio, the concentration of TiO^{+2} is increased due to the low ionic strength of hydrolysis solution, resulting in homogeneous nucleation and particle size distribution of spheres [76].

Additionally, Zeng et al [77] have highlighted that the effect of diverse metal ions existing in the sulfate solution should be also considered to understand TiO_2 powder formation after hydrolysis. Because these trace amount of metal ions could be also present in their complex forms in the solution, which entagle the hydrolysis of the titanium oxide powder, eventually.

Unlike to other samples, samples 3, 8 and 9 reveal severe agglomeration of spheres, resulting irregular morphology. The higher H_2SO_4/TiO_2 (mass/mass) ratio value of samples 8 and 9 (8.41 and 15.33 respectively) leading larger particle formation could explain this result. It is noteworthy to investigate sample 3 separately. Because sample 3 has a maximum solid/liquid ratio and the experiment has been done at 120^0C for 6h. Knowing that at prolonged duration, some amount of solution evaporation is noted during the experiment, an increase of solid/liquid ratio is expected. Therefore, the efficiency of sulfuric acid is believed to weaken since diluted sulfuric acid solution is more powerfull in hydrolysis [76].

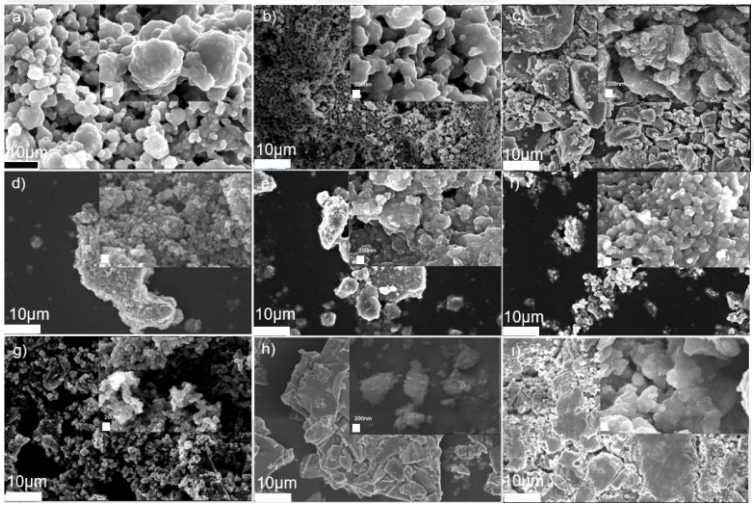

Figure 5.6 : Ti-rich oxide powder's SEM images a) Sampe 1, b) Sample 2, c) Sample 3, d) Sample 4, e) Sample 5, f) Sample 6, g) Sample 7, h) Sample 8, i) Sample 9.

5.3.4. Electrochemical characterizations.

The cyclic voltammogram curvatures of all titanium powders for the first 3 cycle are showed in Fig.5.7. The test has been done at the scanning rate 0.5 mV/s within the potential range of 0.001- 3V. The obtained CV profile shows an apparent pair of reduction/oxidation peaks located at 1.695 and 2.086 V (versus Li/Li^+), which are characteristic for Li^+ insertation and extaraction reactions in anatase lattice [78].

$$TiO_2 + xLi^+ + xe^- \leftrightarrow Li_xTiO_2 \quad (5.10)$$

As stated in the introduction, TiO2 anode material has a particular importance since the lithiation potential is higher than the electrolyte decomposition potential. Therefore, no SEI formation is expected for this material. The latter promotes the reversible cycleability of the electrode material.

Wei et. al [78] have calculated the theoretical capacity of anatase TiO_2 and found 162 mAh/g. Figure 5.6 reveals that samples reveal capacities higher than the theoretical value. Plus, all samples demonstrate relatively low 1st cycle reversibility. The existence of trace element's complex oxide particles (with or without titanium) may cause this outstanding performances. The additional cathodic and anodic peaks (along with those of related to titanium oxide) seen on sample's CV curvatures justify this hypothesis. For instance the additional cathodic peak at 0.59V seen in all samples' CV curves is believed to be related to Fe_2O_3 [34]. Small shift in peak positions is also noted on Fig. 5.7. Which is also believed to be related to the morphological and compositional differences in titanium oxide powders.

To discuss the cycle performance of the TiO_2 powders, the electrode is tested with 50 mA/g current rate in the voltage range of 0.001- 3 V vs Li/Li^+ (Figure 5.8-5.9). It is observed that all samples' capacities get stabilized after initial cycles and their efficiencies reach 99% at the end of 100th cycles.

Figure 5.9 demostrates that, in the first discharge curve of all titanium-oxides is different than others. The first discharge curve has remarkable plateau aroud 1.7V related to the lithiation of TiO_2. Additionally, slope of the discharge curve arround 1.4V and 0.6V are noted for every sample, which may be related to the lithiation of the other metal oxide compounds, such as iron oxide, as discussed previously [34].

Figure 5.8 and Figure 5.10 demonstrates that the highest first initial capacities are achieved in samples 6 and 7. The above emntioned slope changes on the 1st discharge curve are remarkably noted for those 2 sample. The latter may be explained by extent metaloxide content of these TiO_2 samples. This result shows that the spherical morphology, smallest particles size and the narrowest particle size distribution lead in higher electrochemical performances, as expected. Spherical morhology increasing the active contact surface area with the eletrolyte promotes capacity. Plus, the large surface area of small spheres decreases Li^+ ions diffusion.

Both samples reveal similar CV curvatures (Fig 5.7) also substantiates their similar electrochemical behavior versus Li.

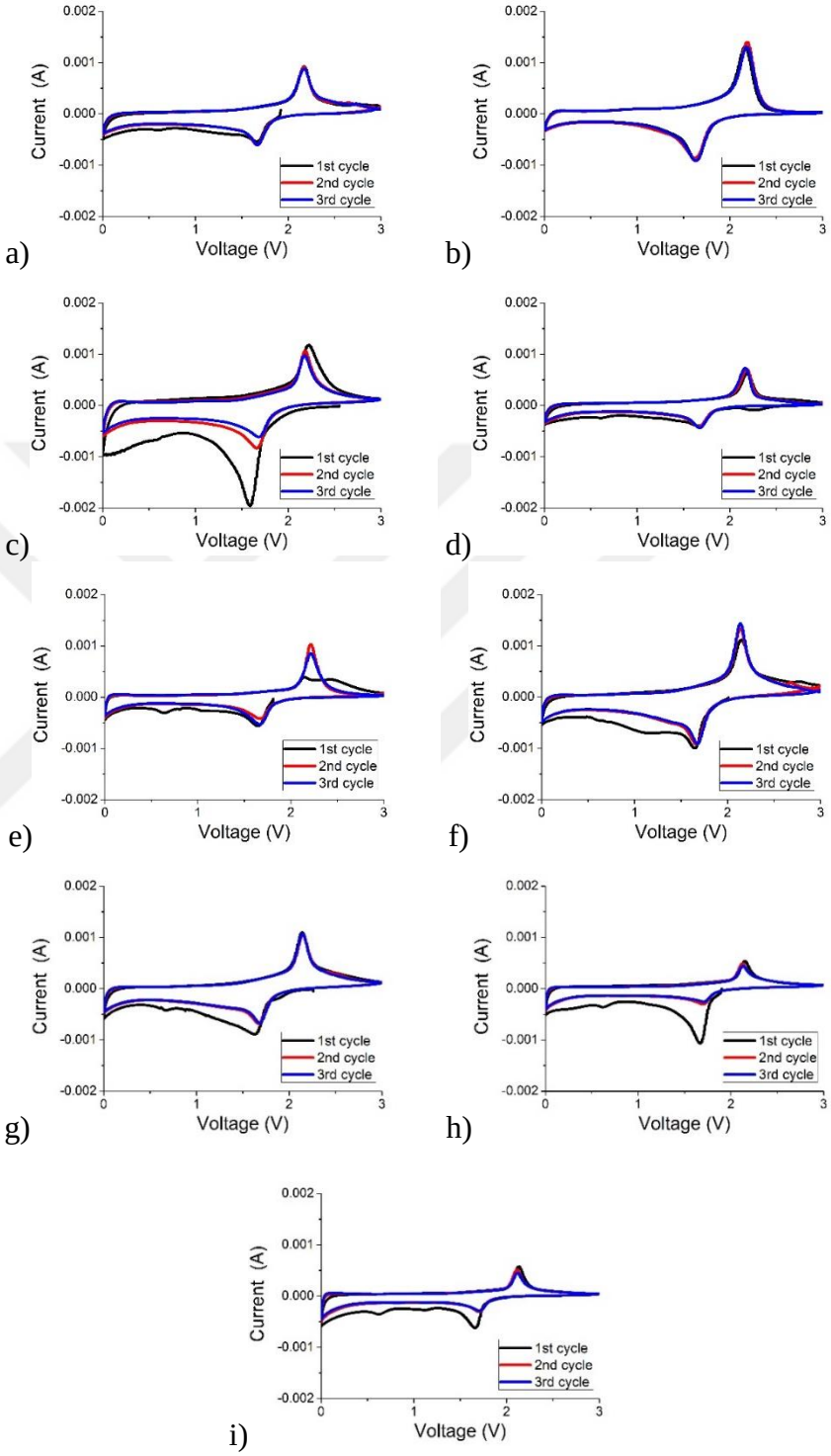

Figure 5.7 : Titanium-rich oxide powder 50 mA/g rate (0.001mV-3V) galvanostatic test results a) sample 1, b) sample 2, c) sample 3, d) sample 4, e) sample 5, f) sample 6, g) sample 7, h) sample 8, i) sample 9.

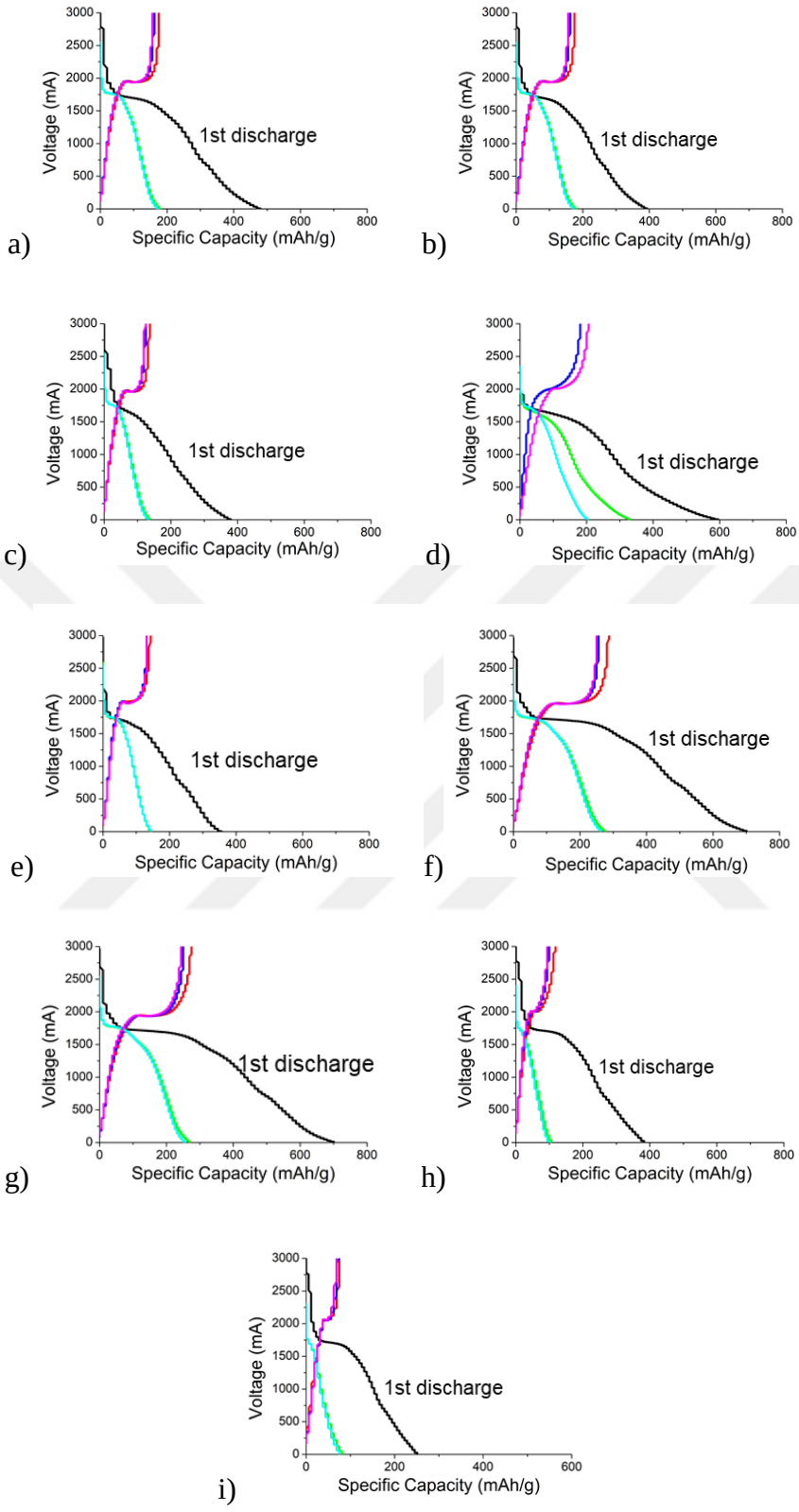

Figure 5.8 : Titanium-rich oxide powder 50 mA/g rate (0.001mV-3V) galvanostatic first 3 cycle results a) sample 1, b) sample 2, c) sample 3, d) sample 4, e) sample 5, f) sample 6, g) sample 7, h) sample 8, i) sample 9.

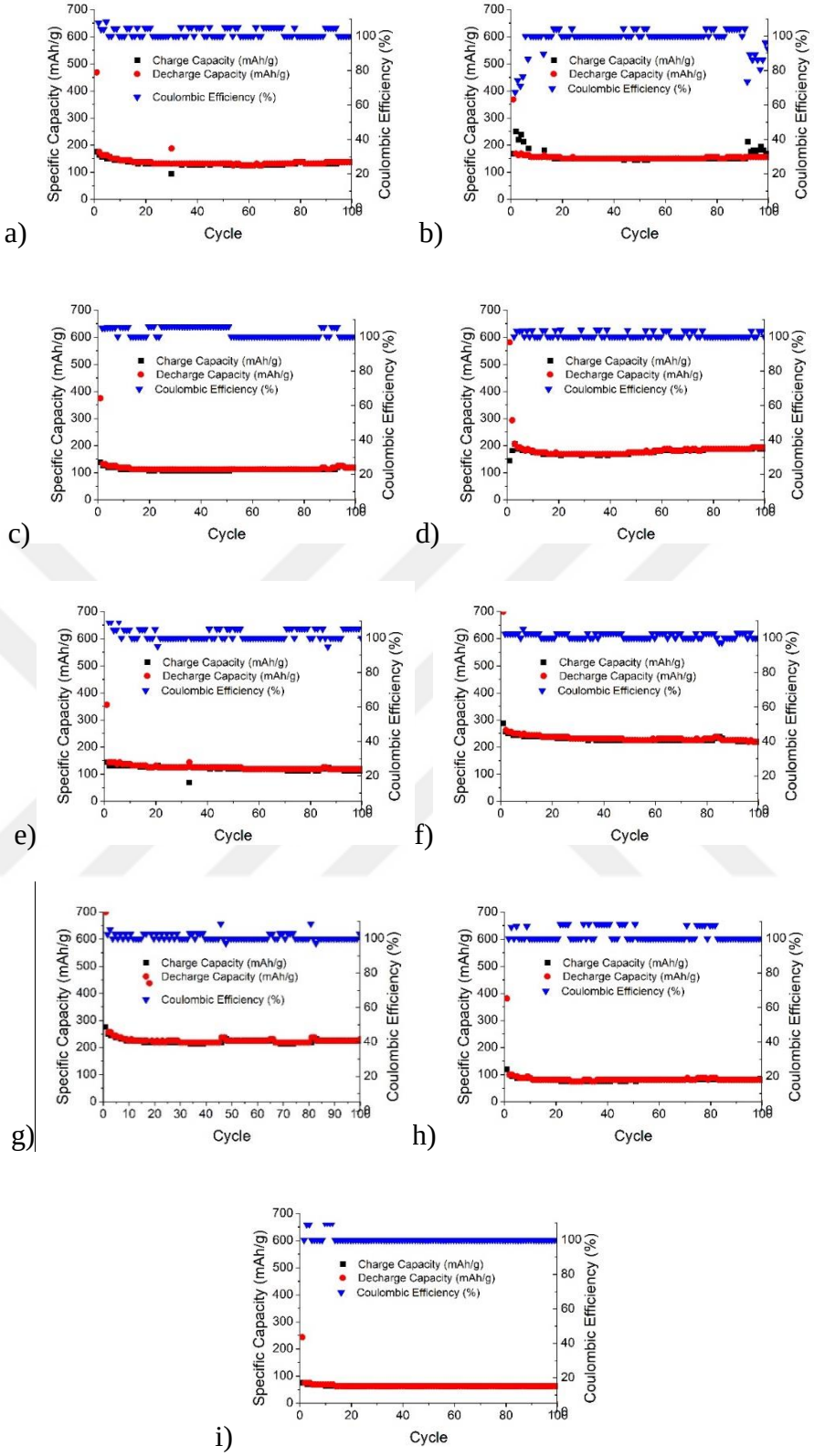

Figure 5.9 : Titanium-rich oxide powder 50 mA/g rate (0.001mV-3V) galvanostatic test results a) sample 1, b) sample 2, c) sample 3, d) sample 4, e) sample 5, f) sample 6, g) sample 7, h) sample 8, i) sample 9.

The performances of samples 3, 8 and 9 having plate-like morphology reveal poor electrochemical performance. The agglomerated particles with limited active surface reaction area is thought to explain this observation. As can be seen the spherical anatase structure is more suitable for Li ion in and out.

5.4 Iron Oxide Production and Characterizations

5.4.1 Taguchi experimental design analysis for Fe recovery

Fe ions dissolved from ferro-titanium alloys have been quantitatively determined by AAS method. Plus, iron ions present in the solution after titanium hydrolysis and after oxalic acid treatment are also determined by AAS method. The results are given in Table 5.7. It is seen that sulfuric acid is an efficienct agent to etch iron ions from ferrotitanium alloy. Plus, small decrease in iron ion concentration in the solution after titanium oxide hydrolysis justifies that some amount of iron is also hydrolyzed with titanium. Finally, very small amount of iron is detected once sulfate solution is treated with oxalic acid. Table 5.7 highlights that oxalic acid is an effective agent to recover iron from the sulfate solution and iron recover efficiency from the leachate is around 70% for all samples.

Table 5.7 : AAS analysis results of iron ions during the production.

Experiment	After leaching AAS(g/L)	After hydrolysis AAS(g/L)	After oxalic acid treatment AAS(g/L)	Iron recovery(%)
1	1.65	1.35	0.23	86
2	1.76	1.4	0.55	68
3	1.58	1.46	0.70	55
4	1.74	1.19	0.69	60
5	1.45	0.70	0.37	74
6	1.83	1.60	0.53	71
7	1.60	1.5	0.77	51
8	1.85	1.25	0.35	81
9	1.88	0.83	0.47	78

Table 5.3 shows the S/N ratios calculated considering Taguchi's “larger is better” approach using Equation 5.1 [70].

Figure 5.10 illustrates the average S/N ratio for each parameter at three levels. Leaching time is found to be the least effective parameter. Therefore, a revised

ANOVA analysis is conducted by pooling this parameter into the error function (Tables 5.8 and 5.9).

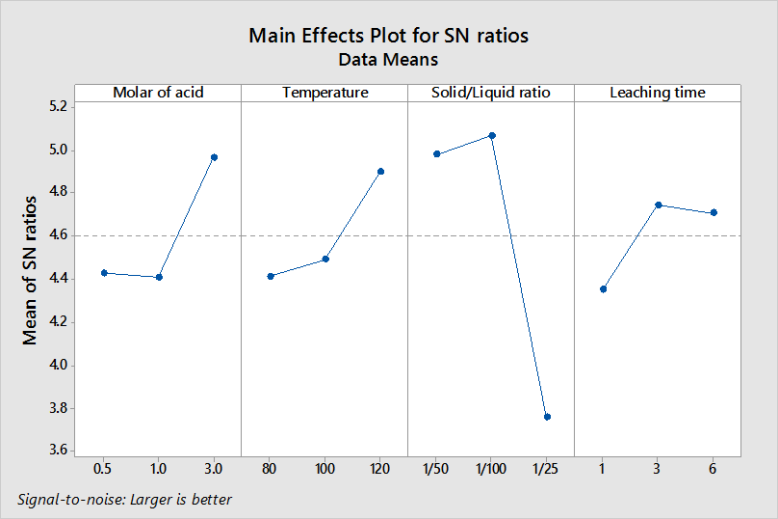

Figure 5.10 : Main effect plot for S/N rations of Fe ion leaching yield .

Table 5.8 : ANOVA analysis of Fe ions leaching efficiency.

Parameter	Degree of freedom	Sum of Square	Mean of Sq
Molarity	2	0.604	0.302
Temperature.	2	0.410	0.205
Solid/Liquid	2	3.204	1.602
Time	2	0.283	1.141
total	8	4.502	

Table 5.9 : Revised ANOVA analysis of Fe ions leaching efficiency.

Parameter	Degree of freedom	Sum of Square	Mean of Sq	F value	Contribution
Molarity	2	0.604	0.302	2.135	7.139
Temperature	2	0.410	0.205	1.449	2.826
Solid/liquid ratio	2	3.204	1.602	11.316	64.878
Error	2	0.283	1.141		
Total	8	4.502			

Fe ions decomposition from ferrotitanium alloy increases in time, then roughly stabilizes. There is no hydrolysis of Fe ions in prolonged duration because Fe-sulfate

ions are more stable at low pH values. Therefore, in experiments conducted longer than 3h (maximum leaching efficiency) no remarkable changes in Fe^{+} ion concentration is found in Fig.5.8 [63].

The effects of temperature and acid molar parameters on iron ion leaching efficiencies are found to be remarkable. Li et. al. have suggested that, elevating temperature improves the surface reaction rate and decreases the viscosity of the liquid phase. Correspondingly, ion diffusion resistance is reduced and mass transfer driving force is enhanced [62]. Moreover, for the acid molar ratio, increase in molarity of the acid in the solution promotes the interaction of sulfate ions with the precursor material (ferrotitanium alloy).

As can be seen in the analysis, the most effective parameter on iron leaching is the solid/liquid ratio. Because an increase in the solid/liquid ratio increases the sulfuric acid leaching efficiency upto a level since more available iron containing precursor material is getting contact with sulfuric acid. Then, further increase in solid content causes inefficient sulfuric acid etching effect, causing lower iron ions' recovery yield [71].

According to the Taguchi analyses, the highest leaching yield is achieved when the experiment is conducted in 3M acid solution (A3) at 120^{o}C (B3) with 1/100 solid/liquid ratio (C2) in 3 hours (D2).

In order to obtain the highest leaching efficiency the optimized Fe ions concentration is calculated using the following equation [70]:

$$u = \frac{T}{n} + \left(\frac{A3}{r} - \frac{T}{n}\right) + \left(\frac{B3}{r} - \frac{T}{n}\right) + \left(\frac{C2}{r} - \frac{T}{n}\right) + \left(\frac{D2}{r} - \frac{T}{n}\right) \tag{5.10}$$

u represents optimum value, T (41.429) denotes the level totals of each parameters in S/N ratios, n the number experiments (9) and r is the number of replications for each parameter (3) in L_9 (3^4). A3, B3, C2 and D2 are selected to be the maximum levels for parameters in order to get maximum Fe ion leach efficiency. The estimated value is found as 4.53 db corresponds to 1.70 g/l Fe ion in the leachate. One additional control experiment is carry out to verify the calculated value of 1.70 g/l. The verification experiment is done and Fe ion concentration is measured to be 1.95 g/l, which is very close to the theoretically calculated value.

To get further understanding about the leaching process of iron ion, additional experiments have been conducted and 5mL of leaching solution is taken out for AAS analysis. To keep solid/liquid ratio as constant, each time additional 5mL sulfuric acid solution at 120^0C is added into the flask.Time dependent Fe ion concentration in the solution justifies our hypothesis(fig.5.11): leaching reaction is very fast for iron in the defined experimental conditions: 3M H_2SO_4, 120^0C, 1/100 solid/liquid ratio at 3h.

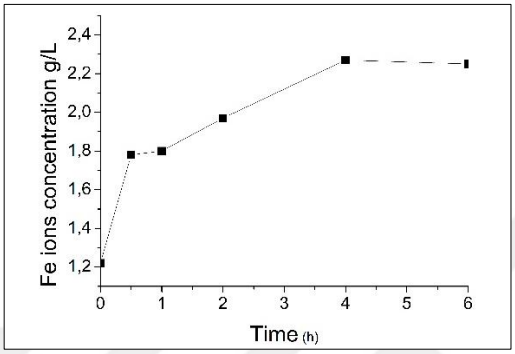

Figure 5.11 : Time dependent Fe ion leaching yield.

5.4.2 Structural, compositional and morphological characterizations

The phase purity and crystallinity of all iron oxide powders are characterized using XRD method, as shown in Figure 5.12. Diffraction peaks well matched to the rhombohedral α-Fe_2O_3 structure (01-089-0599). Additionally, a remarkable slope is noted at low diffraction angles of sample 1, 8 and 9 showing amorphous and/or nanocrystalline particles' presence. The narrow peak and the high intensity of peaks substantiate the existence of crystalline α-Fe_2O_3 particles in all samples.

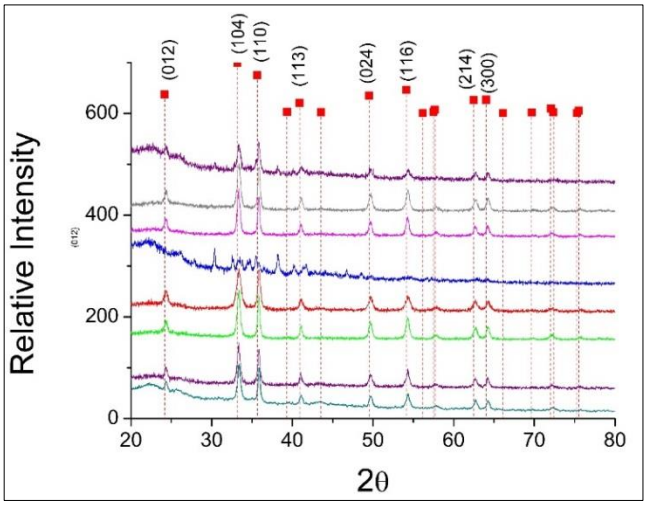

Figure 5.12 : XRD analysis of iron oxide samples.

The EDS analysis results of all iron oxide samples are given in Table 5.10. All samples contain high Fe and O atoms, as expected. In addition, different ratios of Ti, Al, S and Na atoms are found as impurities. Ti and Al atoms are believed to be originated from ferrotitanium alloy. S and Na atoms are thought to be detected as the residues from sulfuric acid leaching and NaOH treatment.

Once iron ions are leached out from the precursor material, the leachate has been treated with oxalic acid to precipitate iron oxalate powders. Ang et. al [81] have stated that iron-oxalate crystallization mainly depends on three parameters: pH of the solution, amount of oxalic acid present in the solution and reaction temperature. In their experimental research, they have found that up to pH 3, the yield of the Fe-oxalate crystallization increases then remains stable at higher pH value. The residues in the leachate such as Co, Mn and Ni are also found to be precipitated in the iron oxalate particles at pH 3. Therefore, in this study the trace amount of impurities are believed to be coprecipitated with iron during the oxalate reaction [71].

Table 5.10 : EDS analysis of iron oxide powder (C atom. at. %).

.Sample	Fe	O	Ti	Al	S	Na
1	38.77	58.23	0.01	0.37	0.66	1.96
2	40.16	50.35	0.01	0.29	2.27	7.17
3	42.37	51.01	0.01	0.05	0	0.15
4	27.87	55.66	0.16	0	0.15	16.16
5	39.29	58.05	0.05	0.38	0.39	1.85
6	46.80	52.90	0.06	0.07	0	0.17
7	51.21	48.29	0.18	0.08	0	0.24
8	40.21	45.12	0.27	0.06	0	14.34
9	49.46	48.57	1.73	0.07	0.01	0.15

The SEM images of the iron oxide powders are given in Figure 5.13. It is seen that all iron oxide powders' have micrometer sizes and rod-like morphologies. These iron oxide powders have been fabricated following the oxalic acid reaction and calcination processes, as defined in the Experimental chapter.

It is noteworthy to claim that pH of the sulfate solution has a particular importance for the efficiency of oxalic treatment. Temperature and concentration of anions and

cations in the solution also affect the oxalic acid reaction mechanism. In this perspective, studies have revealed that SO_4^- and Na^+ ions in the solution that are adsorbed on the surfaces of oxalate crystals support preferrential growth, changing the morphology of the oxalate sample [79]. Indeed, changes in the amount of metal ions is also found to affect the crystallization and growth mechanisms of iron oxalate powders [80].

Ang et. al. have verified this concept experimentally and suggested that, depending on the large differences in their 'ionization abilities', oxalic acid and Fe ions do not react instantly. They have also referred previous studies and highlighted that difference in the solubility, nucleation and growth of oxalate particles in different media, their reaction kinetics, the media (solution) properties and stability of particles are the essential parameters affecting the oxalate morphologies. Therefore, the interaction between the crystallographic planes of FeO_x and solvents defines the morphology of particles [81].

The average width and lengths of nine samples after calcination are given in Table 5.11.

Table 5.11 : Average widths and lengths of the 9 iron oxide samples.

Sample	Average Width(μm)	Average lenght(μm)	Lenght/Widht
1	2.26	10.762	4.76
2	0.74	4.32	5.83
3	0.82	3.56	4.32
4	0.98	4.70	4.79
5	1.61	4.84	3.00
6	1.24	4.69	3.78
7	2.50	6.50	2.60
8	1.20	5.30	4.41
9	1.37	10.00	7.29
Control exp.	1.71	5.38	3.14

These results prove that at 3M H_2SO_4 solution rods with larger diameters have been fabricated (samples 7-8-9). Some micro-cracks have been also noted along the surface of nanorods. Sample 2 shows the least regular morphology whilst sample 6 reveals the best regular rod-like morphology.

An additional SEM analysis has been applied on the iron oxide particles that are fabricated under the control experiment's conditions (3M H_2SO_4, 1/100 solid/liquid ratio, 120^0C, 3h). Figure 5.14 shows SEM images of iron oxalate and iron oxide particles. Results demonstrate that rod-like morphology is related to oxalic acid treatment process. Similar to other nine oxide samples, the iron oxide rod has nano-sized empty spaces in the structure. Thus, the calcination of oxalate particle is believed to form these empty spaces in the rods which are expected to increase the efficiency of the oxide anode material in cycling.

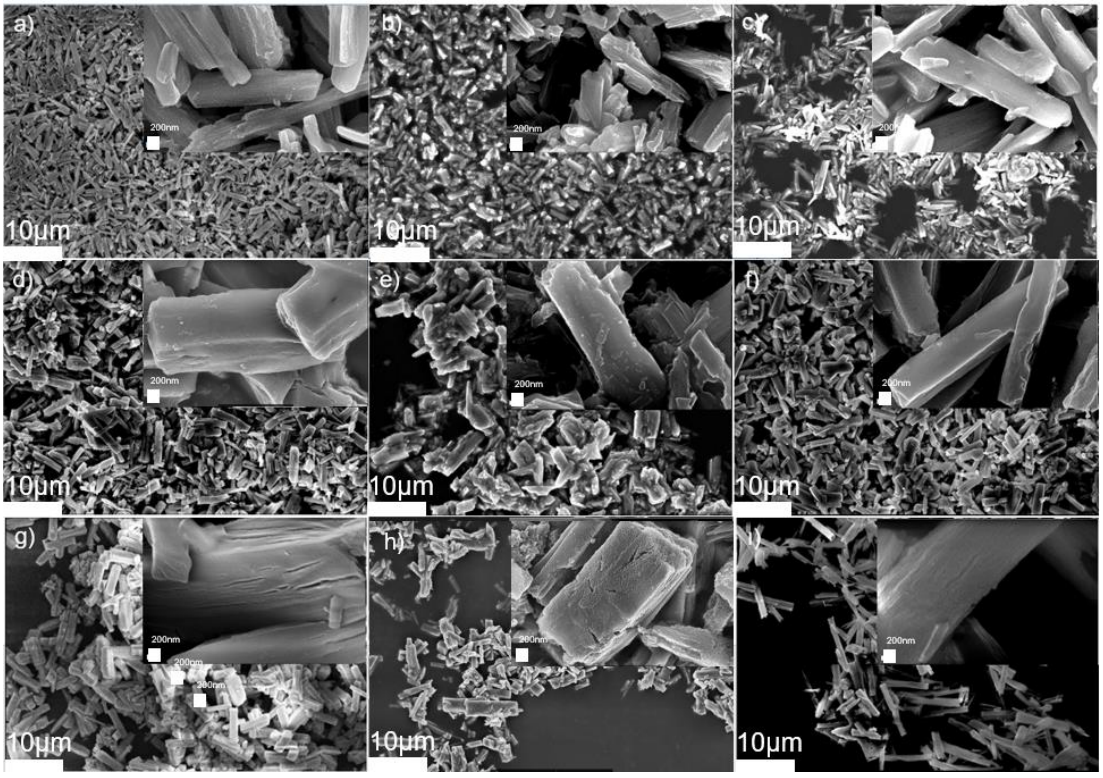

Figure 5.13 : Fe-rich oxide powder's SEM images a) Sample 1, b) Sample 2, c) Sample 3, d) Sample 4, e) Sample 5, f) Sample 6, g) Sample 7, h) Sample 8, i) Sample 9.

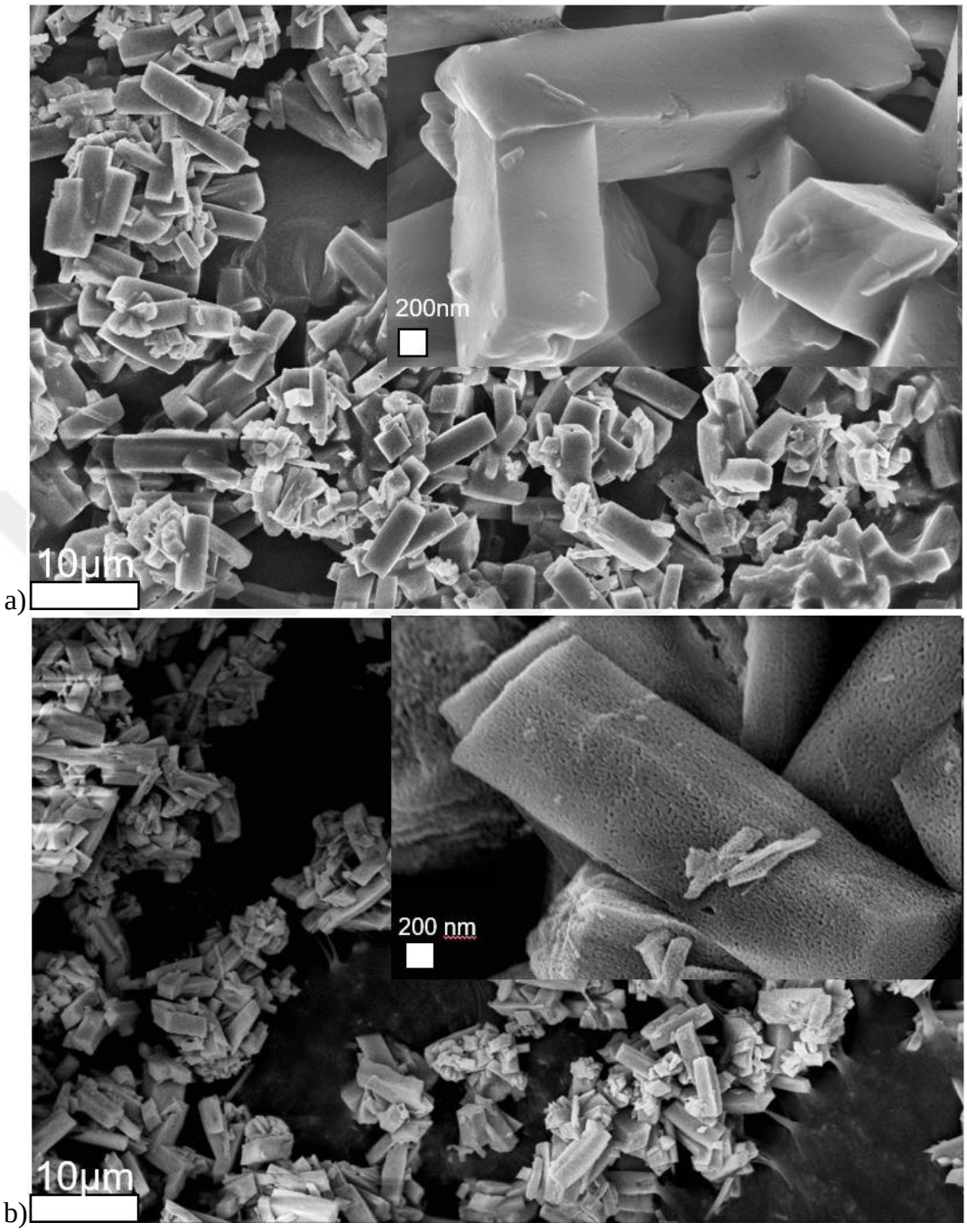

Figure 5.14 : a) Iron oxalate particle surface morphology, b) Iron oxide particle surface morphology.

5.4.3 Electrochemical characterization results of iron oxide powders

The cyclic voltammogram curvatures of all hematite powders for the first 3 cycle are shown in Fig.5.15. The scanning rate has been chosen as 0.5 mV/s and the samples have been cycled between the potential range of 0.001- 3V. It is assumed that there is a considerable difference between the first and the subsequent cycles' curvatures.

The cathodic peaks around 0.5-0.7V are noted for every samples' first discharge reaction. These peaks show the reduction of Fe^{3+} to Fe^{0} and Fe^{3+} to Fe^{2+} , respectively. Additionally, the peak related to the irreversible reductive decomposition of electrolyte to form solid electrolyte interphase layer is also believed to be included in this cathodic peak. An anodic peak is noted about ~1.75 V corresponding to reversible oxidation of iron atoms. In the 2nd cycle the cathodic peak shifts to more positive voltage value due to the polarization of the electrode material. It is believed that the amount of polarization on each sample changes depending on the composition and the morphology of the iron oxide rich particles. The lithiation mechanism of the nano-sized hematite particles are believed to be occurred following equation (5.11).

$$Fe_2O_3 + 6Li^+ + 6e^- \leftrightarrow 3Li_2O + 2Fe^{3+} \qquad (5.11)$$

Figure 5.16 demostrates that, in the first discharge of all iron-oxide sample, small plateau around 1.6 V is noted related to the lithiation of TiO_2 particles as discussed before. All sample remarkable plateau around 0.8-0.5 which show SEI formation on the electrode with lithiation of Fe_2O_3 particles. The slope change around 1V may be realted to the lithiation of metal oxide impurities.

The capacity-cycle performances of all iron oxide samples as anode active materials for LIBs at 50 mA/g current rate in the voltage range of 0.001- 3 V vs Li/Li^+ are given in Figure 5.17. It is observed that capacities of all samples are different and their efficiencies achieve 99% at the end of 100^{th} cycles.

Although the theoretical capacity of hematite is around 1005 mAh/g, the first discharge capacities of the samples are much higher than this value. Possible trace element's complex oxide particles (with or without iron oxide particles) and SEI formation may explain this first cycle extent capacity [31]. Figure 5.16 demonstrate that samples 7 +and 6 reveal the highest initial discharge capacities. Their capacities decrease gradually over cycles. This may be explained by 'electrochemical pulverization' of active particles in cycling [34].

The fact that all samples had different morphological, compositional and structural properties, it is not suprising to achieve different electrochemical performances from each sample [35]. When the capacity results after 50 cycles are examined, samples 1, 4, 6, 7 and 9 show discharge capacities higher than 200 mAh/g.

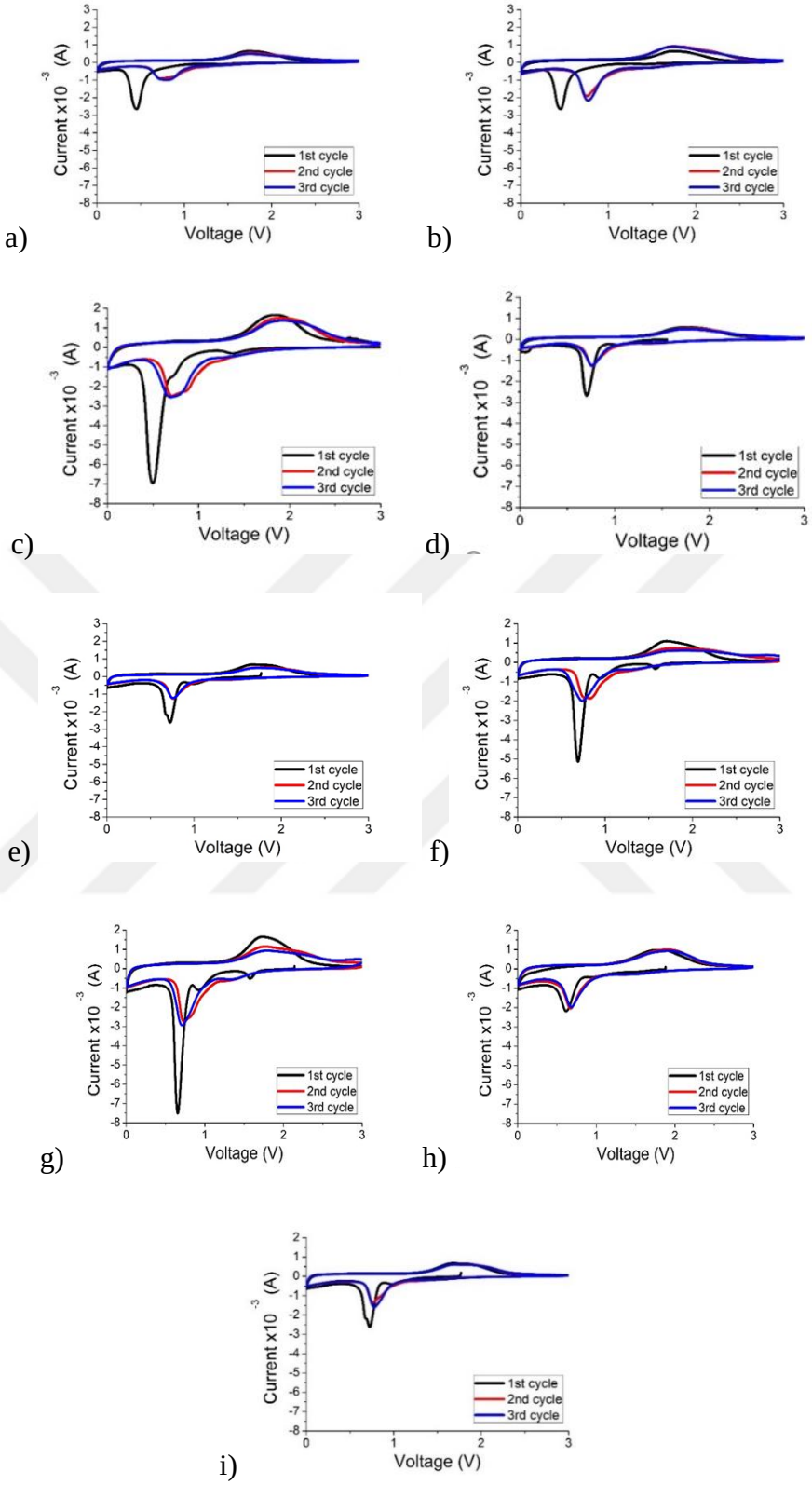

Figure 5.15 : Iron-rich oxide powder 50 mA/g rate (0.001mV-3V) galvanostatic test results a) Sample 1, b) Sample 2, c) Sample 3, d) Sample 4, e) Sample 5, f) Sample 6, g) Sample 7, h) Sample 8, i) Sample 9.

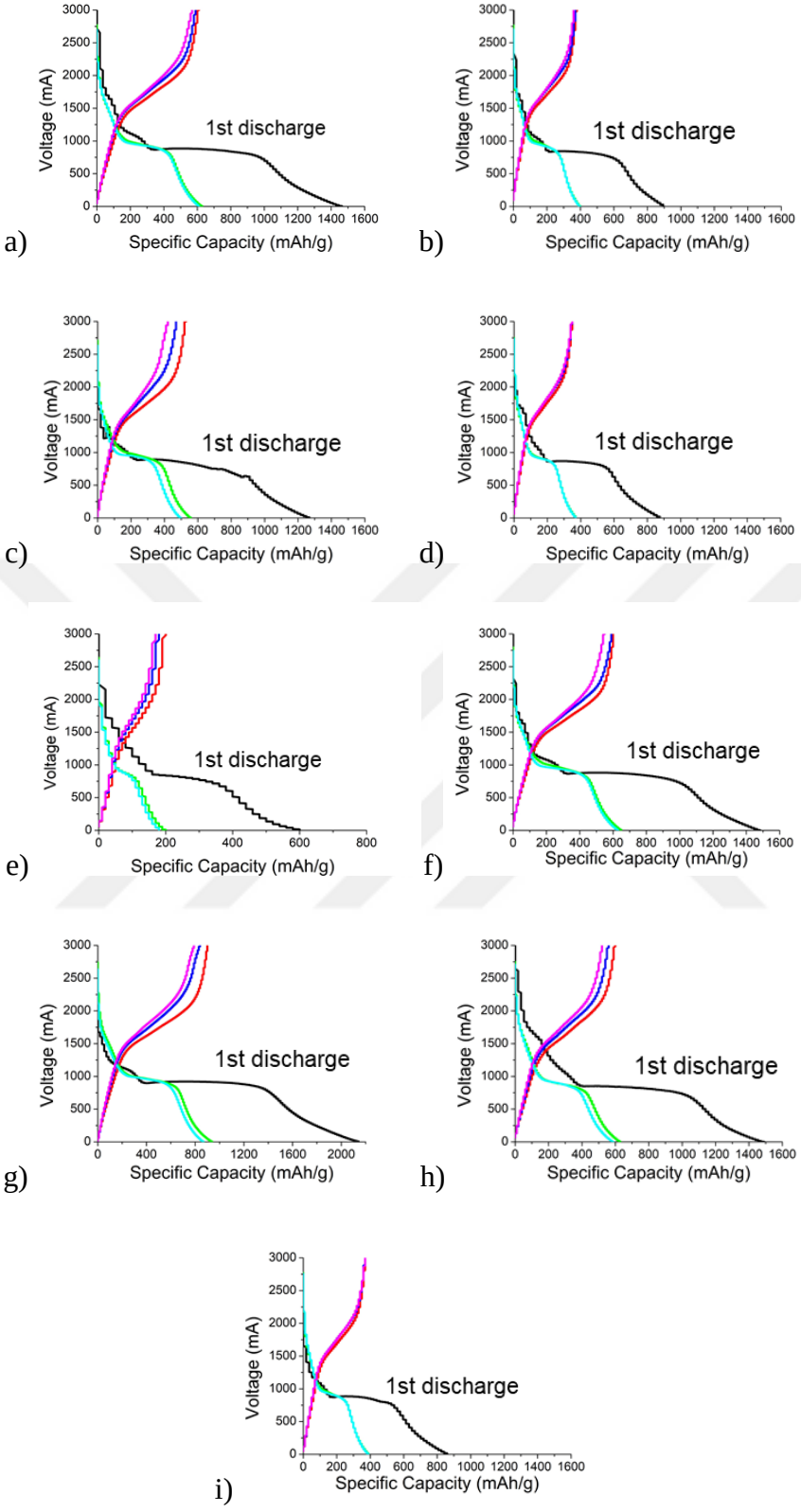

Figure 5.16 : Iron-rich oxide powder 50 mA/g rate (0.001mV-3V) galvanostatic first 3 cycle results a) sample 1, b) sample 2, c) sample 3, d) sample 4, e) sample 5, f) sample 6, g) sample 7, h) sample 8, i) sample 9.

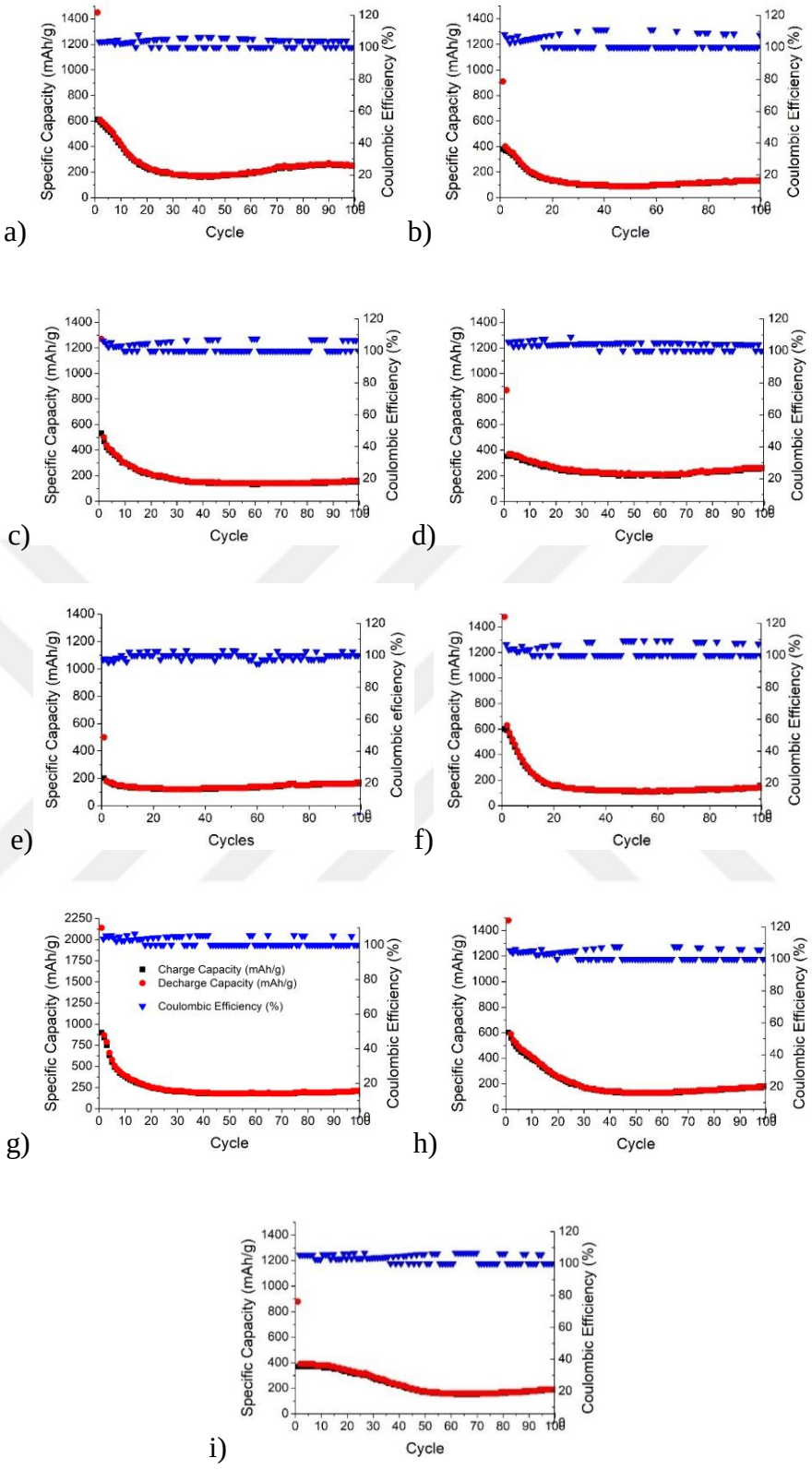

Figure 5.17 : Iron-rich oxide powder 50 mA/g rate (0.001mV-3V) galvanostatic test results a) Sample 1, b) Sample 2, c) Sample 3, d) Sample 4, e) Sample 5, f) Sample 6, g) Sample 7, h) Sample 8, i) Sample 9.

6. CONCLUSION

The approach presented in this thesis is very unique. It unifies principles of extractive metallurgy and powder metallurgy to fabricate new electrode materials for lithium ion batteries. First in literature, in this thesis, by leaching ferro titanium alloy with sulfuric acid, two metal oxide powders (titanium oxide rich and iron oxide rich) are produced. A zero-waste management perspective is followed while desining the experimental procedure. Taguchi design of experiment is utilized to maximize the leaching efficiency of iron ions and the fabrication of titanium oxide powders, independently.

The oxide powders are characterized morphologically, compositionally and structurally. Then, their performances as metal oxide anode materials are investigated. In Taguchi L_9 (3^4) design, temperature, acid molar ratio, solid-liquid ratio and process duration are considered as parameters, and their effects on leaching efficiencies are discussed based on ANOVA analysis results. The AAS results of the leached Fe ions and the mass weights of the produced TiO_2 powders are used in the ANOVA analysis.

(1) The produced metal oxide powders are confirmed to have α-Fe_2O_3 hematite and TiO_2 anatase structure by XRD analysis. It is obtained from SEM analysis that hematite powders have micron size nanorod shape and TiO_2 powders are in spherical form with micron diameter.

(2) Taguchi analysis shows that the effective parameters for Fe ion leaching efficiencies are as follows;

    3 M Acid concentration, 120^0C temperature, 1/100 solid/liquid ratio and 3 h leaching time

(3) Taguchi analysis shows that the effective parameters for titanium oxide powder formation are as follows;

    3 M Acid concentration, 120^0C temperature, 1/100 solid/liquid ratio and 3 h leaching time

(4) During the fabrication of titanium oxide particles out of ferrotitanium alloy first acidic etching then hydrolysis and calcination are applied. Its understood that, the presence of different metal ions (impurities), SO^{4-} and Na^{+} ions in the solution during hydrolysis has a significant effect on the morphology of the final product. The presence of these ions in different proportions is due to the difference in leaching parameters. The calcination temperature is adjusted to achieve anatase crystalline structure.

(5) During the fabrication of iron oxide particles through ferrotitanium alloy first acidic etching then selective precipitation and calcination are used. To selectively precipitate iron from sulfate leachate, oxalic acid treatment is chosen. The sulfuric acid concentration, nucleation and growth of the oxalate particles, oxalate formation kinetics and stability of oxalate particles in different medium are found to be important parameters influencing the last product's morphology. The calcination temperature is also arranged to fabricate hematite crystalline structure.

(6) The possible use of these oxide powders as anode material has been discussed based on galvanostatic test results. The morphology of the metal powders and the existence of impurities in the structure are found to affect the anode performance.

- Among TiO_2 powders, sample 7 (3 M acid concentration, 80^0C 1/25 solid/liquid ratio, 3 h leacing time) performs the highest initial discharge capacity (700mAh/g). the electrode retains 250 mAh/g capacity after 100 cycle. This value is higher than its theoretical capacity. The presence of possible complex oxide particles are believed to elucidate this additional capacity delivered by the electrode. The nanometer-sized spheres of sample 7 with homogeneous morphology explains this outstanding performance.
- Among Fe_2O_3 powders, sample 7 (3 M acid concentration, 80^0C 1/25 solid/liquid ratio, 3 h leacing time) delivers the highest initial capacity (2100mAh/g) but the capacity retention is very low (around 10%). On the other hand, sample 4 delivers 875 mAh/g as the first discharge capacity and retains 35% of its initial discharge capacity after 100^{th} cycles. The unhomogeneous particle size distribution and relatively large particle size of nanorods are considered to be the reson of these performances.

(7) The lithiation kinetic of the oxide samples have revealed that no SEI formation occurs for TiO_2 samples unlike to Fe_2O_3 samples. The number of the peak and their positions change after 1st cycle. The possible formation of complex metal oxide particles (resulted from the reaction of impurities and iron oxide particles) may explain this difference.

REFERENCES

[1] **Tarascon J-M, Armand M.** (2011) Issues and challenges facing rechargeable lithium batteries. In: Materials for Sustainable Energy: A Collection of Peer-Reviewed Research and Review Articles from Nature Publishing Group. World Scientific, pp 171-179

[2] **Díaz-González F**, **Sumper A, Gomis-Bellmunt O, Villafáfila-Robles R.** (2012) A review of energy storage technologies for wind power applications. Renewable and sustainable energy reviews 16 (4):2154-2171

[3] **Wang Y**, **Wu Y, Xing L, Wang Q, Xue X-Y.** (2016) CoMoO4/Fe2O3 core-shell nanorods with high lithium-storage performance as the anode of lithium-ion battery. Journal of Alloys and Compounds 689:655-661

[4] **Shin JY**, **Samuelis D, Maier J.** (2011) Sustained Lithium- Storage Performance of Hierarchical, Nanoporous Anatase TiO2 at High Rates: Emphasis on Interfacial Storage Phenomena. Advanced Functional Materials 21 (18):3464-3472

[5] **Linden D**, **Reddy TB.** (2002) Lithium batteries. D Linden, TB Reddy,"Handbook of Batteries", McGraw-Hill, third edition, New York:14.31-14.55

[6] **Choi NS**, **Chen Z, Freunberger SA, Ji X, Sun YK, Amine K, Yushin G, Nazar LF, Cho J, Bruce PG.** (2012) Challenges facing lithium batteries and electrical double- layer capacitors. Angewandte Chemie International Edition 51 (40):9994-10024

[7] **Cao K**, Jin T, Yang L, Jiao L (2017) Recent progress in conversion reaction metal oxide anodes for Li-ion batteries. Materials Chemistry Frontiers 1 (11):2213-2242

[8] **Khamlich S, Nuru Z, Bello A, Fabiane M, Dangbegnon JK, Manyala N, Maaza M.** (2015) Pulsed laser deposited Cr2O3 nanostructured thin film on graphene as anode material for lithium-ion batteries. Journal of Alloys and Compounds 637:219-225

[9] **Chen M, Li W, Shen X, Diao G.** (2014) Fabrication of core–shell α-Fe2O3@ Li4Ti5O12 composite and its application in the lithium ion batteries. ACS applied materials & interfaces 6 (6):4514-4523

[10] **Park MS.** (2008) Synthesis and characterization of nanostructured electrode materials for rechargeable lithium ion batteries.

[11] **Xu K.** (2014) Electrolytes and interphases in Li-ion batteries and beyond. Chemical reviews 114 (23):11503-11618

[12] **Zhang SS.** (2007) A review on the separators of liquid electrolyte Li-ion batteries. Journal of power sources 164 (1):351-364

[13] **Nitta N, Wu F, Lee JT, Yushin G.** (2015) Li-ion battery materials: present and future. Materials today 18 (5):252-264

[14] **Cho J, Kim YW, Kim B, Lee JG, Park B.** (2003) A breakthrough in the safety of lithium secondary batteries by coating the cathode material with AlPO4 nanoparticles. Angewandte Chemie International Edition 42 (14):1618-1621

[15] **Ohzuku T, Ueda A, Nagayama M.** (1993) Electrochemistry and structural chemistry of LiNiO2 (R3m) for 4 volt secondary lithium cells. Journal of The Electrochemical Society 140 (7):1862-1870

[16] **Martha SK, Haik O, Zinigrad E, Exnar I, Drezen T, Miners JH, Aurbach D.** (2011) On the thermal stability of olivine cathode materials for lithium-ion batteries. Journal of the Electrochemical Society 158 (10):A1115-A1122

[17] **Bruce P, áRobert Armstrong A, Gitzendanner R.** (1999) New intercalation compounds for lithium batteries: layered LiMnO 2. Journal of Materials Chemistry 9 (1):193-198

[18] **Wang R, He X, He L, Wang F, Xiao R, Gu L, Li H, Chen L.** (2013) Atomic structure of Li2MnO3 after partial delithiation and re- lithiation. Advanced Energy Materials 3 (10):1358-1367

[19] **Lee M-J, Lee S, Oh P, Kim Y, Cho J.** (2014) High performance LiMn2O4 cathode materials grown with epitaxial layered nanostructure for Li-ion batteries. Nano letters 14 (2):993-999

[20] **Antolini E.** (2004) LiCoO2: formation, structure, lithium and oxygen nonstoichiometry, electrochemical behaviour and transport properties. Solid State Ionics 170 (3-4):159-171

[21] **Yamada A, Chung S-C, Hinokuma K.** (2001) Optimized LiFePO4 for lithium battery cathodes. Journal of the electrochemical society 148 (3):A224-A229

[22] **Choi D, Wang D, Bae I-T, Xiao J, Nie Z, Wang W, Viswanathan VV, Lee YJ, Zhang J-G, Graff GL.** (2010) LiMnPO4 nanoplate grown via solid-state reaction in molten hydrocarbon for Li-ion battery cathode. Nano letters 10 (8):2799-2805

[23] **Lloris J, Vicente CP, Tirado J.** (2002) Improvement of the electrochemical performance of LiCoPO4 5 V material using a novel synthesis procedure. Electrochemical and solid-state letters 5 (10):A234-A237

[24] **Sobkowiak A, Roberts MR, Younesi R, Ericsson T, Häggström L, Tai C-W, Andersson AM, Edström K, Gustafsson Tr, Björefors F.** (2013) Understanding and controlling the surface chemistry of LiFeSO4F for an enhanced cathode functionality. Chemistry of Materials 25 (15):3020-3029

[25] **Li Y, Zhou Z, Gao X, Yan J.** (2006) A novel sol–gel method to synthesize nanocrystalline LiVPO4F and its electrochemical Li intercalation performances. Journal of Power Sources 160 (1):633-637

[26] **Zhang W**-J. (2011) A review of the electrochemical performance of alloy anodes for lithium-ion batteries. Journal of Power Sources 196 (1):13-24

[27] **Zaghib K, Simoneau M, Armand M, Gauthier M.** (1999) Electrochemical study of Li4Ti5O12 as negative electrode for Li-ion polymer rechargeable batteries. Journal of Power Sources 81:300-305

[28] **Poizot P, Laruelle S, Grugeon S, Dupont L, Tarascon J.** (2000) Nano-sized transition-metal oxides as negative-electrode materials for lithium-ion batteries. Nature 407 (6803):496

[29] **Liang C, Gao M, Pan H, Liu Y, Yan M.** (2013) Lithium alloys and metal oxides as high-capacity anode materials for lithium-ion batteries. Journal of Alloys and Compounds 575:246-256

[30] **Li H, Huang X, Chen L.** (1999) Anodes based on oxide materials for lithium rechargeable batteries. Solid State Ionics 123 (1-4):189-197

[31] **Muraliganth T, Murugan AV, Manthiram A.** (2009) Facile synthesis of carbon-decorated single-crystalline Fe3O4 nanowires and their application as high performance anode in lithium ion batteries. Chemical communications (47):7360-7362

[32] **Zhang J, Yao Y, Huang T, Yu A.** (2012) Uniform hollow Fe3O4 spheres prepared by template-free solvothermal method as anode material for lithium-ion batteries. Electrochimica Acta 78:502-507

[33] **Reddy M, Yu T, Sow C-H, Shen ZX, Lim CT, Subba Rao G, Chowdari B.** (2007) α- Fe2O3 nanoflakes as an anode material for Li- ion batteries. Advanced Functional Materials 17 (15):2792-2799

[34] **Lin Y-M, Abel PR, Heller A, Mullins CB.** (2011) α-Fe2O3 nanorods as anode material for lithium ion batteries. The Journal of Physical Chemistry Letters 2 (22):2885-2891

[35] **Xu X, Cao R, Jeong S, Cho J.** (2012) Spindle-like mesoporous α-Fe2O3 anode material prepared from MOF template for high-rate lithium batteries. Nano letters 12 (9):4988-4991

[36] **Jiao F, Bao J, Bruce PG.** (2007) Factors influencing the rate of Fe2O3 conversion reaction. Electrochemical and Solid-State Letters 10 (12):A264-A266

[37] **Pan X.** (2015) Tin Nanoparticles Encapsulated in Hollow TIO2 Spheres as High Performance Anode Materials for Li-Ion Batteries.

[38] **Sudant G, Baudrin E, Larcher D, Tarascon J-M.** (2005) Electrochemical lithium reactivity with nanotextured anatase-type TiO 2. Journal of Materials Chemistry 15 (12):1263-1269

[39] **Jung H-G, Oh SW, Ce J, Jayaprakash N, Sun Y-K.** (2009) Mesoporous TiO2 nano networks: Anode for high power lithium battery applications. Electrochemistry Communications 11 (4):756-759

[40] **Borghols WJ, Lützenkirchen-Hecht D, Haake U, Chan W, Lafont U, Kelder EM, van Eck ER, Kentgens AP, Mulder FM, Wagemaker M.** (2010) Lithium storage in amorphous TiO2 nanoparticles. Journal of The Electrochemical Society 157 (5):A582-A588

[41] **Das SK, Bhattacharyya AJ.** (2011) Influence of mesoporosity and carbon electronic wiring on electrochemical performance of anatase titania. Journal of The Electrochemical Society 158 (6):A705-A710

[42] **Zhu P, Wu Y, Reddy M, Nair AS, Chowdari B, Ramakrishna S.** (2012) Long term cycling studies of electrospun TiO 2 nanostructures and their composites with MWCNTs for rechargeable Li-ion batteries. Rsc Advances 2 (2):531-537

[43] **Shin J-Y, Joo JH, Samuelis D, Maier J.** (2012) Oxygen-deficient TiO2− δ nanoparticles via hydrogen reduction for high rate capability lithium batteries. Chemistry of Materials 24 (3):543-551

[44] **Hu YS, Kienle L, Guo YG, Maier J.** (2006) High lithium electroactivity of nanometer- sized rutile TiO2. Advanced Materials 18 (11):1421-1426

[45] **Baudrin E, Cassaignon S, Koelsch M, Jolivet J-P, Dupont L, Tarascon J-M.** (2007) Structural evolution during the reaction of Li with nano-sized rutile type TiO2 at room temperature. Electrochemistry communications 9 (2):337-342

[46] **Bach S, Pereira-Ramos J, Willman P.** (2010) Investigation of lithium diffusion in nano-sized rutile TiO2 by impedance spectroscopy. Electrochimica Acta 55 (17):4952-4959

[47] **Zhang X**, Hou Z, Li X, Liang J, Zhu Y, Qian Y (2016) MoO2 nanoparticles as high capacity intercalation anode material for long-cycle lithium ion battery. Electrochimica Acta 213:416-422

[48] **Krishnan SG, Ab Rahim MH, Jose R.** (2016) Synthesis and characterization of MnCo2O4 cuboidal microcrystals as a high performance psuedocapacitor electrode. Journal of Alloys and Compounds 656:707-713

[49] **Zhang J, Yu A.** (2015) Nanostructured transition metal oxides as advanced anodes for lithium-ion batteries. Science bulletin 60 (9):823-838

[50] **Aşık B.** (2013) Ultrasonik Sprey Piroliz (usp) Yöntemi İle Nano Yapılı Kurşun Oksit Üretimi Ve Karakterizasyonu. Fen Bilimleri Enstitüsü,

[51] **Li W, Fries DP, Malik A.** (2004) Sol–gel stationary phases for capillary electrochromatography. Journal of Chromatography A 1044 (1-2):23-52

[52] **Xio**ng X, Wang Z, Wu F, Li X, Guo H. (2013) Preparation of TiO2 from ilmenite using sulfuric acid decomposition of the titania residue combined with separation of Fe^{3+} with EDTA during hydrolysis. Advanced Powder Technology 24 (1):60-67

[53] **Lütjering G, Williams JC.** (2007) Titanium. Springer Science & Business Media,

[54] **Liu Y, Qi T, Chu J, Tong Q, Zhang Y.** (2006) Decomposition of ilmenite by concentrated KOH solution under atmospheric pressure. International Journal of Mineral Processing 81 (2):79-84

[55] **Amer A.** (2002) Alkaline pressure leaching of mechanically activated Rosetta ilmenite concentrate. Hydrometallurgy 67 (1-3):125-133

[56] **Nayl A, Ismail I, Aly H.** (2009) Ammonium hydroxide decomposition of ilmenite slag. Hydrometallurgy 1 (98):196-200

[57] **Zhang Y, Qi T, Zhang Y.** (2009) A novel preparation of titanium dioxide from titanium slag. Hydrometallurgy 96 (1-2):52-56

[58] **Van Dyk JP, Vegter NM, Pistorius PC.** (2002) Kinetics of ilmenite dissolution in hydrochloric acid. Hydrometallurgy 65 (1):31-36

[59] **Chernet T.** (1999) Effect of mineralogy and texture in the TiO 2 pigment production process of the Tellnes ilmenite concentrate. Mineralogy and petrology 67 (1-2):21-32

[60] **Liu S-s, Guo Y-f, Qiu G-z, Jiang T.** (2013) Preparation of Ti-rich material from titanium slag by activation roasting followed by acid leaching. Transactions of Nonferrous Metals Society of China 23 (4):1174-1178

[61] **Jia L, Liang B, Lü L, Yuan S, Zheng L, Wang X, Li C.** (2014) Beneficiation of titania by sulfuric acid pressure leaching of Panzhihua ilmenite. Hydrometallurgy 150:92-98

[62] **Li Z, Wang Z, Li G.** (2016) Preparation of nano-titanium dioxide from ilmenite using sulfuric acid-decomposition by liquid phase method. Powder Technology 287:256-263

[63] **Liang B, Li C, Zhang C, Zhang Y.** (2005) Leaching kinetics of Panzhihua ilmenite in sulfuric acid. Hydrometallurgy 76 (3-4):173-179

[64] **Das G, Pranolo Y, Zhu Z, Cheng C.** (2013) Leaching of ilmenite ores by acidic chloride solutions. Hydrometallurgy 133:94-99

[65] **Biswas R, Mondal M.** (1987) A study on the dissolution of ilmenite sand. Hydrometallurgy 17 (3):385-390

[66] **Vasquez R, Molina A.** Leaching of ilmenite and pre-oxidized ilmenite in hydrochloric acid to obtain high grade titanium dioxide. In: 17th International metallurgical & materials conference proceedings: METAL, 2008.

[67] **Gasik M.** (2013) Handbook of ferroalloys: theory and technology. Butterworth-Heinemann,

[68] **Taguchi G.** (1990) Introduction to Quality Engineering, Tokyo. Asian Productivity Organization

[69] **Ross PJ.** (1996) Taguchi techniques for quality engineering: loss function, orthogonal experiments, parameter and tolerance design.

[70] **Keleş O.** (2009) An optimization study on the cementation of silver with copper in nitrate solutions by Taguchi design. Hydrometallurgy 95 (3-4):333-336

[71] **Liu J-j, Hu G-r, Du K, Peng Z-d, Wang W-g, Cao Y-b.** (2014) The new technique on separation of Cr and Fe as well as Ni-Co-Mn impurity in leaching sulfate solution of ferrochrome alloy. Russian Journal of Non-Ferrous Metals 55 (6):533-537

[72] **Guo Y-G, Hu Y-S, Maier J.** (2006) Synthesis of hierarchically mesoporous anatase spheres and their application in lithium batteries. Chemical Communications (26):2783-2785

[73] **Polleux J, Pinna N, Antonietti M, Hess C, Wild U, Schlögl R, Niederberger M.** (2005) Ligand functionality as a versatile tool to control the assembly behavior of preformed titania nanocrystals. Chemistry–A European Journal 11 (12):3541-3551

[74] **Wang W, Liu Y, Xue T, Li J, Chen D, Qi T.** (2015) Mechanism and kinetics of titanium hydrolysis in concentrated titanyl sulfate solution based on infrared and Raman spectra. Chemical Engineering Science 134:196-204

[75] **Tian C, Huang S, Yang Y.** (2013) Anatase TiO2 white pigment production from unenriched industrial titanyl sulfate solution via short sulfate process. Dyes and Pigments 96 (2):609-613

[76] **Sathyamoorthy S, Moggridge GD, Hounslow MJ.** (2001) Particle formation during anatase precipitation of seeded titanyl sulfate solution. Crystal Growth & Design 1 (2):123-129

[77] **Zeng F, Luo D, Zhang Z, Liang B, Yuan X, Fu L.** (2016) Study on the behavior of sulfur in hydrolysis process of titanyl sulfate solution. Journal of Alloys and Compounds 670:249-257

[78] **Wei H, Rodriguez EF, Hollenkamp AF, Bhatt AI, Chen D, Caruso RA.** (2017) High Reversible Pseudocapacity in Mesoporous Yolk–Shell Anatase TiO2/TiO2 (B) Microspheres Used as Anodes for Li- Ion Batteries. Advanced Functional Materials 27 (46):1703270

[79] **Sudakar C, Subbanna G, Kutty T.** (2003) Effect of anions on the phase stability of γ-FeOOH nanoparticles and the magnetic properties of gamma-ferric oxide derived from lepidocrocite. Journal of Physics and Chemistry of Solids 64 (12):2337-2349

[80] **Sudakar C, Subbanna GN, Kutty TN.** (2002) Synthesis of acicular hydrogoethite (α-FeOOH· x H 2 O; 0.1< x< 0.22) particles using morphology controlling cationic additives and magnetic properties of maghemite derived from hydrogoethite. Journal of Materials Chemistry 12 (1):107-116

[81] **Ang WA, Gupta N, Prasanth R, Madhavi S.** (2012) High-performing mesoporous iron oxalate anodes for lithium-ion batteries. ACS applied materials & interfaces 4 (12):7011-7019

CURRICULUM VITAE

Name Surname **:**Eren İNEL

Place and Date of Birth **:** Eskişehir 08/08/1993

E-Mail **:** inel17@itu.edu.tr

EDUCATION **:**

- **B.Sc.** **:** 2016 Yıldız Teknik Üniversitesi Metalurji ve Malzeme Mühendisliği